Mantle sources of kamafugitic magmas: insights from partial melting experiments on phlogopite clinopyroxenite and clinopyroxene glimmerite

Francesca Innocenzi<sup>1,2,3\*</sup>, Isra S. Ezad<sup>3,4</sup>, Sara Ronca<sup>1</sup>, Samuele Agostini<sup>2</sup>, Michele Lustrino<sup>1,5</sup>, Svyatoslav Shcheka<sup>3,4</sup>, Stephen F. Foley<sup>3,6</sup>

<sup>1</sup> Dipartimento di Scienze della Terra, Sapienza Università di Roma, P.le A. Moro, 5, 00185 Roma, Italy
<sup>2</sup> Istituto di Geoscienze e Georisorse – CNR, Via Moruzzi, 1, 56124, Roma, Italy

<sup>6</sup> Research School of Earth Sciences, Australian National University, Canberra ACT2601, Australia Corresponding author at: Dipartimento di Geoscienze, University of Padova, Via Giovanni Gradenigo, 6, 35131, Padova, Italy. E-mail address: francesca.innocenzi@unipd.it

Keywords: mantle metasomatism, glimmerite, clinopyroxenite, partial melting experiments

## **Abstract**

Earth's lithospheric mantle is dominated (usually >90% vol.%) by a nominally volatile-free mineral paragenesis with peridotitic composition. The remaining lithologies are typically hydrous and/or carbonate-bearing assemblages (the latter stable mostly at P >2 GPa), representing the products of mantle metasomatism with or without involvement of subduction. Despite their importance, the modal compositions of these metasomes are poorly constrained, likely containing hydrous phases (amphibole and/or phlogopite), coupled with accessory phases, such as apatite, ilmenite, rutile and/or carbonates. These assemblages are usually considered to be the source of unusual magmas, in particular ultrapotassic compositions, especially kamafugites (K<sub>2</sub>O-rich, commonly ultracalcic, basic/ultrabasic lithologies). To evaluate if partial melting of such metasomes could effectively produce kamafugites, we performed partial melting experiments at 2.7 and 5 GPa, and 1200 °C to 1550 °C on clinopyroxenites variably enriched in phlogopite, olivine and accessory phases (apatite, oxides, titanite), and on a clinopyroxene glimmerite (with apatite and magnetite).

At low degrees of melting, the glasses show extremely high  $TiO_2$  (<15 wt.%), CaO (<18 wt.%) and  $P_2O_5$  (<7.4 wt.%), coupled with low  $SiO_2$  (>21.6 wt.%), as accessory minerals are the principal contributors in the melting reactions. Although there are no known natural counterparts for these

<sup>&</sup>lt;sup>3</sup> School of Natural Sciences, Macquarie University, North Ryde, New South Wales 2109, Australia.

<sup>&</sup>lt;sup>4</sup> School of Earth Sciences, University of Western Australia, Perth, Western Australia 6009, Australia

<sup>&</sup>lt;sup>5</sup> Istituto di Geologia Ambientale e Geoingegneria – CNR, c/o Dipartimento di Scienze della Terra, Sapienza Università di Roma, P.le A. Moro, 5, 00185 Roma, Italy

low-degree melt compositions, they may play a key role in re-fertilization events in the upper mantle. At increased degrees of partial melting ( $\sim$ 50 to  $\sim$ 90%), the experimental melts approach the compositions of silica-poor, potassic/ultrapotassic and ultracalcic rocks. Indeed, experimental glasses share several geochemical similarities with natural kamafugites, partially overlapping for most of the major oxides. Clinopyroxene- and phlogopite-rich lithologies, variably enriched in olivine and accessory phases (apatite, oxides, titanite) probably occur as veins pervading the lithospheric peridotitic matrix, and their partial melting, especially at high degrees, may be a plausible explanation for the genesis of SiO<sub>2</sub>-poor, K<sub>2</sub>O- and CaO-rich compositions.

### 1 Introduction

Continental intraplate igneous rocks may exhibit unusual compositions diverging strongly from typical partial melts generated from volatile-free peridotitic sources, leading to the formation of extreme compositions, such as ultra-alkaline rocks (including nephelinites, leucitites, lamproites) strongly ultrabasic compositions (e.g. melilitites, kimberlites), carbonatites and (ultramafic) lamprophyres (e.g. Foley et al. 2008). Despite their rarity, these igneous compositions are very important because their genesis can shed light on how upper mantle anatexis works (e.g. Foley et al. 2025).

The unusual features of ultrapotassic lithologies in terms of petrography, mineral chemistry, whole-rock geochemistry and isotopic ratios cannot be reconciled with derivation from a classical four-phase lherzolitic mantle, whose melting produces tholeiitic to mildly alkaline basaltic melts, with Na<sub>2</sub>O + K<sub>2</sub>O lower than 5-6 wt.% and usually <2 wt.% K<sub>2</sub>O (Green, 1970; Frey et al. 1978). For this reason, the petrogenesis of ultrapotassic lithologies is often linked to the presence of metasomatic mantle assemblages (e.g. Foley et al. 2008; Kiseeva et al. 2017; Lustrino et al. 2020; 2024; Innocenzi et al. 2024a; 2024b; Shu et al. 2024; Foley et al. 2025). Crustal recycling and fluids released by subducting slabs may cause refertilization events in the form of chromatographic reactions, resulting in the development of mantle reservoirs characterized by variable enrichment in incompatible elements (both major oxides and trace elements) and by isotope signatures that strongly deviate from those typical of peridotitic mantle rocks. The mineralogy of the metasomatic rocks as well as the nature and the physical state of the metasomatic agents are not yet completely understood (e.g. Roden and Murthy, 1985; Kiseeva et al. 2017; Förster et al., 2017; Foley and Ezad, 2024).

Several petrological investigations have focused on ultramafic xenoliths occasionally entrained in ultrapotassic magmas to constrain their possible mantle sources. They commonly display peculiar mineral assemblages such as clinopyroxenites and glimmerites, examples of which are found along the western branch of the East African Rift (Lloyd et al. 1985; Link et al. 2008; Innocenzi et al. 2024a).

Obviously, being found as xenoliths in ultrapotassic magmas, these lithologies cannot be used as direct constraints to identify the mineralogical and chemical characteristics of the mantle sources of the host rocks. Petrological experiments on mantle rocks other than peridotite are now abundant, despite being mostly confined to anhydrous pyroxenites (e.g. Keshav et al. 2004; Kogiso and Hirschmann, 2001; Borghini et al. 2017), eclogites (e.g. Klemme et al. 2002; Spandler et al. 2008), and aiming to constrain the effects of interaction between metasomatic agents and a peridotitic matrix (e.g. Yaxley and Green, 1998; Förster et al. 2017; 2019). High pressure partial melting experiments on hydrous ultramafic rocks such as phlogopite-bearing clinopyroxenite and/or glimmerites (Lloyd et al. 1985; Sweeney et al. 1993; Funk and Luth, 2013; Foley et al. 2022; Foley and Ezad, 2024) result in very variable ranges of glass compositions. It is important to emphasize that experiments carried out at pressures >3 GPa are particularly rare (Foley et al. 2022; Foley and Ezad, 2024; Shu et al. 2024) or have concentrated on delineating subsolidus phases, not on melt compositions (Konzett, 1997; Konzett et al., 1997). Beside this relative paucity of experiments at pressures at which many ultrapotassic melts are thought to form, the mineral assemblages used for these melting experiments are often very similar and less extreme when compared to glimmerites. For example, many starting materials contained amphibole (like in most of the experiments from Foley et al. 2022 and Foley and Ezad, 2024) or orthopyroxene (e.g. Shu et al. 2024). Moreover, the effect of accessory phases is commonly overlooked. Only in few cases have oxides, rutile, sphene and/or apatite been considered, and the effects of different combinations of these minor phases is still poorly constrained (Lloyd, 1985; Funk and Luth, 2013; Foley et al. 2022; Foley and Ezad, 2024).

A previous investigation (Innocenzi et al. 2024c), based on near-liquidus experiments (1-2 GPa and 1250-1380 °C) on different kamafugite compositions tried to reconstruct the paragenesis of the melting assemblage of Ugandan, Italian and Brazilian kamafugites, proposing a major role for partial melting of clinopyroxene- and phlogopite-rich paragenesis, with minor olivine and accessory phases (as titanite, apatite and Fe-Ti-oxides).

To verify this hypothesis, in this study we carried out partial melting experiments at 2.7-5 GPa and 1200-1550 °C on three hydrous ultramafic rocks, ranging from phlogopite-bearing clinopyroxenite (± olivine) to clinopyroxene-bearing glimmerite. The aim of this experimental study is to characterise the melt compositions generated from these hydrous ultramafic rocks, comparing them with data on natural kamafugites. Two different pressures of 2.7 and 5 GPa have been selected for these experiments as kamafugites crop out in different geodynamic settings (*i.e.* craton edges, along old mobile belts and on active compressive margins), resulting in variable lithospheric thickness and melting depths. In particular, the estimated mantle sources of the three known kamafugite

occurrences range from less than 90 km to  $\sim$ 180 km, corresponding to  $\sim$ 2.7 to 5.0-5.5 GPa (Innocenzi et al. 2025).

## 2 Starting materials

The starting materials of this study were chosen on the results of the near-liquidus experiments (Innocenzi et al. 2024c) carried out on four natural kamafugites from three geographical areas (Toro Ankole Province, western branch of the East African rift in Uganda; Alto Paranaiba Igneous Province in Brazil; Cupaello and San Venanzo volcanoes, Intra-Apennine Province in central Italy). The minerals crystallized in near-liquidus runs allowed Innocenzi et al. (2024c) to hypothesize their presence in the source of primary kamafugite magma and, therefore, they could represent the main mineralogical components of the melting assemblages.

On this basis, we modelled the hypothetical sources for the three studied volcanic provinces where kamafugite rocks occur: Toro Ankole (TA; Uganda), Alto Paranaiba Igneous Province (APIP; Brazil) and the Intra-Apennine Province (IAP; Italy; Tappe et al. 2003; Innocenzi et al 2025). The compositions of the starting materials are reported in Table 1. The three assemblages are a phlogopite clinopyroxenite + apatite + ilmenite + magnetite + titanite for TA, an olivine clinopyroxenite + phlogopite + apatite + ilmenite for APIP, and a clinopyroxene glimmerite + apatite + magnetite for IAP. Experiments were not doped with additional H<sub>2</sub>O or CO<sub>2</sub>.

For sake of clarity, it should be noted that the near-liquidus experiments (Innocenzi et al. 2024c) for the two IAP lavas from San Venanzo and Cupaello returned different results. Olivine was observed only in San Venanzo runs and not in Cupaello due to the different bulk composition of the two natural samples (with San Venanzo showing higher MgO than Cupaello; Lustrino et al. 2020, 2025; Innocenzi et al. 2025). Therefore, the reconstruction of the IAP starting material for this study was based both on the San Venanzo and Cupaello experimental results of Innocenzi et al. (2024c) and on the partial melting model (Innocenzi et al. 2025) based on mass balance calculations (File Repository 3, <a href="https://doi.org/10.5880/fidgeo.2025.025">https://doi.org/10.5880/fidgeo.2025.025</a>). No olivine is present in the mixture and phlogopite reaches 55% (Table 1).

Starting materials were prepared by mixing hand-picked minerals from the following natural rocks: Ti-poor phlogopite from a glimmerite xenolith from Kimberley (South Africa); Ti-rich phlogopite, clinopyroxene, titanite and ilmenite from a pyroxene-bearing glimmerite from the western branch of the East African Rift (Uganda); olivine and magnetite from a lherzolite xenolith from Lanzarote (Spain). Apatite comes from Durango (Mexico).

Rock samples were previously disintegrated using a selective fragmentation (SelFrag) instrument at Macquarie University (Sydney, Australia). Mineral compositions were determined by XRD

(Panalytical Aeris; Cobalt X-ray source, operating at 40kV, 15Ma, with one rotation per second) and by SEM-EDS analyses (Zeiss EVO MA15). These compositions are reported in Table 2.

## 3.1 Experimental strategy

A set of five partial melting experiments were run at 2.7 GPa on each of the three starting materials. To better constrain the olivine-free assemblages, further experiments on the TA and IAP source assemblages were performed at 5 GPa. Temperature ranged from 1200 to 1400 °C at intervals of 50 °C for the 2.7 GPa experiments, and from 1200 to 1550 °C at 50 °C intervals for the 5 GPa experiments.

The 2.7 GPa melting experiments were conducted using a GUKO ½ inch rapid quench end-loaded piston cylinder (Ezad et al., 2023), whereas the runs at 5 GPa were performed in a Voggenreiter 1000 ton multi-anvil press with a Walker module. Both apparatuses were housed at the School of Natural Sciences at Macquarie University. For the piston cylinder experiments, natural CaF<sub>2</sub>-MgO-graphite assembly and B-type thermocouple (Pt<sub>30</sub>Rh<sub>70</sub>-Pt<sub>6</sub>Rh<sub>94</sub>) were employed. The reaction albite = jadeite + quartz was used for the pressure calibration (Holland, 1980) and a friction correction of 20% was applied. For the multi-anvil experiments, an 18/11 Cr-doped MgO assembly with a stepped graphite heater was employed. Temperature was measured using D-type thermocouple (W<sub>97</sub>Re<sub>3</sub>-W<sub>75</sub>Re<sub>25</sub>) and monitored with a Eurotherm 350H controller. Pressure calibration followed the reactions of quartz/coesite (2.97 GPa; Bohlen and Boettcher, 1982) and coesite/stishovite transformation (8.7 GPa; Zhang et al. 1996).

Powders of the three starting materials were loaded in graphite capsules wrapped with a Pt foil (25 µm in thickness). The graphite capsules were made using a Roland MDX-540 mill. All experiments were first compressed to the desired pressure (2.7 or 5 GPa) and subsequently heated to the target temperature, held for 12 hours at 2.7 GPa and 10 hours at 5 GPa, quenched to room temperature by cutting power to the graphite and decompressed over several hours (3-16 hours). A summary of the run conditions and resulting phases can be found in Table 2.

# 3.2 Analytical methods

The recovered samples were embedded in epoxy resin and polished to a 1 µm diamond finish. Quantitative chemical analyses of the mineral phases and glasses, coupled with chemical mapping, were acquired using a SEM Zeiss EVO MA15, equipped with an EDS detector (Oxford Ultim Max 100), at Macquarie GeoAnalytical Laboratories (MQGA; Macquarie University). The instrument operates at 20 kV and a working distance of 12 mm. The quality of the quantitative results has been documented by Shu et al. (2024), demonstrating good agreement (<2% error) between the EDS measurements and the data obtained from an electron microprobe (JEOL HAX 8530F WDS), at the University of Tasmania.

Mainly due to the low SiO<sub>2</sub> and high MgO content of the compositions, the glasses do not always quench, producing glassy patches with several small needle microliths. This results in challenges to polish the experimental glasses and find sufficiently large areas to analyse chemical compositions from. This problem is known in literature (e.g. Shu et al. 2024), and often results in chemical analyses of glasses with low totals. To be sure that the analyses of experimental glasses with low totals were not related to the EDS technique, some analyses were repeated at the Laboratorio di Microanalisi of University of Florence and Istituto di Geoscienze e Georisorse – CNR, using a JEOL JXA-8230 Electronic Microprobe, equipped with five WDS (wave-length dispersive) crystal spectrometers, obtaining similar results (*i.e.* low major oxide totals; Appendix 1).

High quality scanning electron microphotographs were collected using a Teneo FEI–Field Emission Scanning Electron Microscope (FESEM) at MQGA fitted with Bruker XFlash 6-30 EDS detectors, working at 15 kV, with a beam current of 11 nA, a spot size of 1-2 nm and a working distance of 10 mm. FESEM maps are shown in Figs. 2 to 6

#### 4 Results

The experimental results are reported separately for each of the three starting materials. Table 2 summarises the experimental conditions and the resulting paragenesis for each run. Abundances of each phase have been estimated by mass balance (Appendix 1).

All the glass and mineral data for each experiment are given in Appendix 1. Average compositions, together with standard deviation and the number of analyses, for each mineral phase and recovered glasses are reported in Tables 3 and 4 for experiments conducted at 2.7 GPa and in Tables 5 and 6 for experiments at 5 GPa. Major oxides are reported in wt.%, following the journal's rules, albeit the International System of Units would require mass %.

4.1 Experiments on a phlogopite clinopyroxenite + apatite + ilmenite + magnetite + titanite (Toro Ankole Volcanic Province)

## 4.1.1 Experiments at 2.7 GPa

TA experiments at 1200 °C produced the same mineral assemblage as the starting material, indicating sub-solidus conditions (Fig. 1). A measurable amount of melt ( $\sim$ 20 wt.%) appeared at 1250°C, visible as quenched needles (Fig. 2a-c), characterised by very low SiO<sub>2</sub> content (29.6 wt.%; Table 3). This glass is anomalously enriched in TiO<sub>2</sub> (10.7 wt.%), CaO (14.7 wt.%), K<sub>2</sub>O (4.3 wt.%) and P<sub>2</sub>O<sub>5</sub> (4.6 wt.%; Table 3 and Appendix 1), reflecting the large contribution of titanite and apatite.

At 1300 °C the degree of partial melting increases to  $\sim$ 37 wt.% (see map in Appendix 1). Clinopyroxene, phlogopite, apatite and ilmenite are still present. These minerals are joined by peritectic olivine characterised by high Fo (0.83) and slight lime enrichment (CaO = 0.76 wt.%; Table 4), formed as consequence of the incongruent melting of phlogopite. The glass composition remains

strongly ultrabasic ( $SiO_2 = 33.5 \text{ wt.\%}$ ), but its  $TiO_2$  and CaO content decrease to 7.3 wt.% and 9.3 wt.%, respectively, while  $K_2O$  increases to 6.2 wt.% (Table 3 and Appendix 1).

At 1350 °C olivine is no longer present and all the accessory phases (apatite, ilmenite, magnetite and titanite) have melted out (Fig. 1). Only minimal traces of phlogopite (~4 wt.%) and large amounts of clinopyroxene (33 wt.%) are still found. The area occupied by glass reaches ~60 wt.% of the experimental charge (Fig. 2d-e). Compared to the 1300 °C experiment, the 1350 °C glass composition shows a slight enrichment in  $SiO_2$  (36.6 wt.%), similar  $TiO_2$  (7.1 wt.%), lower  $K_2O$  (4.1 wt.%) and higher CaO (15.0 wt.%).

The highest temperature experiment at 1400 °C yields a melt fraction of ~90 wt.%, with clinopyroxene (~10 wt.%) remaining as the only residual mineral (Table 4). The glass remains ultrabasic ( $SiO_2 = 40.9$  wt.%), ultrapotassic ( $K_2O = 3.6$  wt.% and  $K_2O/Na_2O = 7$ ) and reaches the highest CaO content (16.4 wt.%).

### 4.1.2 Experiments at 5 GPa

In contrast to what is observed at 2.7 GPa, at 5 GPa, the experiment carried out at 1200 °C approaches near-solidus conditions, with ~1 wt.% of melt (Fig. 3a-c), which was impossible to analyse due to the presence of quenched needles within the small glassy patches (Fig. 1). Beside perovskite, which is present in place of titanite, the mineral assemblage is the same of the starting material (Fig. 3a).

At 1250 °C, the degree of partial melting reaches ~20 wt.%, with glass concentrated along the capsule border. The mineral paragenesis of this experiment is composed of clinopyroxene, phlogopite, tschermakitic amphibole ( $Al_2O_3 = 18.5$  wt.%, FeO = 12.2 wt.%, MgO = 8.7 wt.% and CaO = 17.1 wt.%), perovskite, apatite and ilmenite (Table 6). The glass composition is strongly ultrabasic ( $SiO_2 = 26.7$  wt.%), with high  $TiO_2$ ,  $K_2O$  and  $P_2O_5$  (10.2, 5.5 and 5.2 wt.%, respectively).

At 1350 °C, the degree of partial melting remains low (~30 wt.%), and the melt is mainly concentrated along the grain boundaries (Appendix 1). Clinopyroxene, phlogopite, ilmenite and more abundant tschermakitic amphibole (14 wt.%) are observed in this run ( $Al_2O_3 = 19.9$  wt.%, FeO = 8.4 wt.%, MgO = 13.6 wt.% and CaO = 13.4 wt.%; Table 6). Experimental glass at 1350 °C is strongly ultrabasic (SiO<sub>2</sub> = 24.4 wt.%), enriched in TiO<sub>2</sub>, CaO, K<sub>2</sub>O and P<sub>2</sub>O<sub>5</sub> (12.2, 11.2, 5.3 and 6.6 wt.%, respectively).

The 1400° C experiment is characterised by only ~2 wt.% phlogopite, ~40 wt.% of clinopyroxene and ~58 wt.% glass (Fig. 3d). The glass is slightly richer in  $SiO_2$  (34.9 wt.%), poorer in  $P_2O_5$  (1.9 wt.%) and similar in terms of  $TiO_2$  and  $K_2O$  contents compared to those analysed in the lower temperature experiments (Table 5).

Experiments at 1450 °C, 1500 °C and 1550 °C contained 64, 72 and 85 wt.% glass, respectively (Fig. 1). Clinopyroxene is the only liquidus mineral phase (Appendix 1). Glasses at 1450 and 1500 °C exhibit similar compositions ( $SiO_2 = 36.3$  and 37.2 wt.%,  $TiO_2 = 7.2$  and 7.3 wt.%, and CaO = 15.8 and 15.7 wt.%). The glass at 1550 °C remains ultrabasic ( $SiO_2 = 40.5$  wt.%) and ultrapotassic ( $K_2O = 3.0$  wt.% and  $K_2O/Na_2O = 6$ ), also having high CaO (17.8 wt.%) and  $TiO_2$  (5.2 wt.%). No olivine was found in the TA experiments at 5 GPa.

4.2 Experiments on a clinopyroxene glimmerite + apatite + magnetite (Intra-Apennine Province)

### 4.2.1 Experiments at 2.7 GPa

At 1200 °C no glass was detected, but the occurrence of incongruent melting of phlogopite is indicated by the presence of ~2 wt.% olivine (Fig. 1). Increasing the temperature to 1250 °C results in ~15 wt.% melt production (Fig. 4a-b), with the glass showing ultrabasic composition (SiO<sub>2</sub> = 31.2 wt.%) and enrichment in  $K_2O$  (5.2 wt.%),  $P_2O_5$  (5.5 wt.%) and  $TiO_2$  (5.9 wt.%; Table 3). All apatite and magnetite melted out, leaving only phlogopite (~35 wt.%) and clinopyroxene (~38 wt.%). Olivine (~10 wt.%) is also present in the recovered experiment highlighted by chemical and mineralogical mapping (Fig. 4a), but due to its small size no quantitative analyses could be obtained.

At 1300 °C (Appendix 1), the melt increases to ~30 wt.%, coexisting with ~10 wt.% olivine, ~34 wt.% clinopyroxene and 26 wt.% phlogopite. Olivine is enriched in MgO ( $Fo_{86}$ ), with 0.38 wt.% CaO (Table 4). The higher proportion of melt results in an increase in  $SiO_2$  (34.1 wt.%) and  $K_2O$  (7.2 wt.%) in the glass, as clinopyroxene joins the melting process and the amount of melting phlogopite increases. On the other hand, CaO decreases (down to 11.2 wt.%) together with  $P_2O_5$ , as the effect of accessory phases dilutes these oxides in the melt composition.

At 1350 °C the degree of partial melting reaches ~70 wt.% and phlogopite is exhausted, while ~10 wt.% clinopyroxene is still observed (Fig. 4c-d). Olivine (21 wt.%) shows higher MgO (Fo<sub>92</sub>) and CaO (0.43 wt.%). In the 1400 °C experiment, melt and olivine reach a modal abundance of ~85 wt.% and ~15 wt.%, respectively. Olivine composition is comparable to that observed in the previous experiment (Fo<sub>92</sub>). The glasses in the 1400 °C experiments show slightly higher SiO<sub>2</sub> (42.0 wt.%), TiO<sub>2</sub> (4.4 wt.%) and CaO (14.7 wt.%), when compared to the 1350 °C glass (40.8 wt.%, 4.2 wt.% and 13.4 wt.%, respectively), but also lower  $K_2O$  and  $P_2O_5$ , down to 4.5 wt.% and 1.1 wt.%. The evolving glass compositions results from the increasing amount of clinopyroxene contributing to the melt (up to 40 wt.%).

### 4.2.2 Experiments at 5 GPa

At 1200 °C, the extent of melting is low, yielding ~3 wt.% glass (Fig. 5a-b) and small crystals of olivine (~2 wt.%) (Fig. 5c). With increasing temperature to 1250 and 1350 °C, the degree of partial melting

increases only to 5 wt.% (Fig. 1). There is, however, a slightly higher amount of olivine (~3 wt.%) and intergranular quenched needles may have been lost during polishing. The paragenesis recovered from both experiments is composed of ~40 wt.% clinopyroxene, ~50 wt.% phlogopite, ~1 wt.% magnetite and ~1 wt.% apatite. Due to the small amount of glassy patches in both the 1250 and 1350 °C runs, it was impossible to obtain reliable quantitative analyses.

By 1400 °C, the melt fraction drastically increases to ~43 wt.% (Fig. 5d). Olivine reaches 10 wt.% and coexists with ~2 wt.% tschermakite ( $Al_2O_3 = 20.8$  wt.%, FeO = 6.2 wt.%, MgO = 17.4 wt.% and CaO = 10.0 wt.%; Table 8), ~38 wt.% clinopyroxene and ~7 wt.% phlogopite. The glass is higher in SiO<sub>2</sub> (37.9 wt.%) and  $K_2O$  (8.9 wt.%), coupled with lower TiO<sub>2</sub>, CaO and  $P_2O_5$  (Table 6).

With increasing temperature, the degree of melting reaches ~80 wt.% at 1450 °C, ~85 wt.% at 1500 °C and 90 wt.% at 1550 °C (Fig. 1). The melt compositions show a quite uniform content of  $SiO_2$  (42.3 and 42.1 wt.%),  $TiO_2$  (2.5 and 2.1 wt.%) and CaO (12.0 and 11.9 wt.%) as the melt approaches the composition of the bulk mixture. With temperature increasing from 1450 to 1550 °C,  $P_2O_5$  and  $K_2O$  slightly decrease with the increasing melting degree (from 5.9 wt.% to 4.8 wt.% and from 1.2 wt.% to 0.6 wt.%, respectively). In the 1450 °C experiment, ~5 wt.% olivine is still present (see map in Appendix 1), together with ~10 wt.% clinopyroxene, while at 1500 and 1550 °C only clinopyroxene (15 and 10 wt.%, respectively) still persists (Table 6).

As in the 2.7 GPa experiments, olivine compositions show an increase in MgO and a decrease in FeO (Fo<sub>82</sub> at 1350 °C, to Fo<sub>94</sub> at 1450 °C). The full set of analyses is reported in Table 6.

4.3 Experiments on an olivine clinopyroxenite + phlogopite + apatite + ilmenite (Alto Paranaiba Igneous Province)

## 4.3.1 Experiments at 2.7 GPa

The APIP experiments have been conducted only at 2.7 GPa (Table 2). Due to the composition of the starting materials and the lower modal abundance of phlogopite, this sample showed the lowest degree of melting at any given temperature. At 1200 °C the sample was subsolidus, while ~23 wt.% melt appears at 1250°C (Fig. 1). In the 1250 °C experiment, apatite melted out, while ~43 wt.% clinopyroxene, ~8 wt.% phlogopite, ~25 wt.% olivine and <1 wt.% ilmenite were still observed. The initial melt exhibits a strongly ultrabasic composition ( $SiO_2 = 27.7$  wt.%), roughly overlapping with TA and IAP runs (Table 3 and Fig. 7), but  $TiO_2$ , MgO and CaO are much higher (12.2 wt.%, 11.2 wt.% and 16.5 wt.%, respectively). At 1300 °C, the melt fraction increases up to ~31 wt.% (Appendix 1), showing a slightly higher  $SiO_2$  content than that in the TA run at the same temperature (33.1 wt.%), but similar  $TiO_2$  (9.2 wt.%), CaO (12.8 wt.%), K<sub>2</sub>O (5.7 wt.%) and P<sub>2</sub>O<sub>5</sub> (2.6 wt.%). Accessory phases (apatite and ilmenite) melted out, leaving only ~23 wt.% clinopyroxene, ~25 wt.% olivine and ~5 wt.% phlogopite. Olivine content slightly increased due to the incongruent melting of phlogopite. At

1350 °C, the melt fraction reaches ~50 wt.%, with phlogopite, olivine and clinopyroxene still abundant in the residuum (Table 4; Fig. 6a-c). The 1400 °C experiment contains ~69 wt.% melt (Fig. 6d-e), joined by ~21 wt.% olivine and ~10 wt.% clinopyroxene. The increasing modal amount of clinopyroxene participating to the partial melting, at same percentage of phlogopite and accessory phases (apatite and magnetite), resulted in an increasing  $SiO_2$  (from 36.1 to 41.0 wt.%) and MgO in the glass (from 11.6 to 15.4 wt.%). For the same reason, the FeO,  $K_2O$  and  $P_2O_5$  contents decrease (from 9.1 to 5.9 wt.%, from 3.7 to 3.2 wt.% and from 2.0 to 1.3 wt.%, respectively; Table 3).

In all the runs, olivine shows almost uniform composition (Table 4), although a trend of slightly increasing MgO and decreasing FeO (from Fo<sub>84</sub> at 1250 °C to Fo<sub>92</sub> at 1400 °C) can be observed. CaO remains quite uniform (0.2-0.4 wt.% in the 1250 °C, 0.4 wt.% in the 1300 °C, 0.1-0.7 wt.% in the 1350 °C and 0.3-0.6 wt.% in the 1400 °C).

### **5 Discussion**

High-pressure and high-temperature experiments conducted in this study highlight that partial melting of phlogopite clinopyroxenites and clinopyroxene-bearing glimmerites produces  $SiO_2$ -poor and CaO- and  $K_2O$ -rich compositions overlapping those of natural kamafugites. Furthermore, the results indicate that accessory phases can strongly influence the geochemical composition of the resulting melt, in particular  $TiO_2$  or  $P_2O_5$  contents, which are strongly dependent from the amount of titanite, ilmenite and apatite.

## 5.1 Comparison of natural and experimental compositions

In the following sections, experimental melt compositions are compared to natural kamafugites (references in Appendix 1), which represent volcanic rocks with ultrabasic to basic and potassic to ultrapotassic compositions, characterised by high CaO and variable incompatible trace element enrichment, with the common feature of having primary kalsilite as groundmass phase (Innocenzi et al., 2025). Rocks classified as kamafugites in literature show a wide compositional spread, even when belonging to the same volcanic area or district. The large geochemical variability of kamafugites is likely related to heterogeneous lithospheric mantle sources (Innocenzi et al. 2025).

Natural kamafugites display a wide range of Mg# (from 57 to 93) as well as a large spectrum of major oxide contents. Beside Cupaello lavas, which are interpreted to be evolved samples (Lustrino et al. 2025), little evidence of fractionation has been found in other worldwide kamafugites (Melluso et al. 2008; Rosenthal et al. 2009; Guarino et al. 2013; Lustrino et al. 2020; Innocenzi et al. 2024a, 2024b, 2025).

Natural and synthetic compositions are plotted in Harker diagrams for selected major oxides vs.  $SiO_2$  in Fig. 7 (experiments carried out at 2.7 GPa) and Fig. 8 (experiments at 5 GPa). Further diagrams are presented in Appendix 1. Here, clear trends in experimental glasses with increasing

melting degree are outlined. The melts formed at the lowest temperatures (1250-1350 °C) have low  $SiO_2$ , very high  $TiO_2$  and  $P_2O_5$ , likely due to the partial or complete melting of the accessory phases (titanite, apatite and Fe-Ti-oxides in TA, apatite and ilmenite in APIP, and apatite and magnetite in IAP), while only low amounts of the major phases contribute to the melt. These low-degree melts do not match the compositions of kamafugites or of any other natural melts. At higher temperatures (1350-1400 °C) and consequently larger degrees of partial melting (50-90 wt.%) the experimental melts resemble the natural kamafugites for most of the major oxides (Figs. 7 and 8). However, the  $FeO_{tot}$  contents of experimental melts for all three provinces are slightly lower than natural counterparts, possibly indicating minor FeO loss during the experiments (FeO<sub>tot</sub> in ~90% of the experiments is lower than 1.2 wt.%).

Toro Ankole kamafugites show variable compositional features together with a large spectrum of igneous products in general. Indeed, kamafugitic compositions are replaced by carbonatitic tuffs moving from South to North of the region (e.g. Eby et al., 2009; Zartner, 2010). Moreover, different lithologies (*i.e.* kamafugites, leucitites, nephelinites and olivine-bearing melilitites) with strong compositional similarities have been identified in the TA districts (e.g. Rosenthal et al. 2009; Muravyeva et al. 2014). The minor differences recorded among the samples are supposed to derive from a strongly metasomatized lithospheric mantle characterised by significant heterogeneity, also at short lateral scales. Different abundances of clinopyroxene, phlogopite and carbonate in the source may explain all the rock compositions recorded in TA (Innocenzi et al. 2024a). Furthermore, variable degrees of melting and of interaction with the surrounding mantle matrix may also contribute to explain the observed geochemical diversity (e.g. Rosenthal et al. 2009; Muravyeva et al. 2014; Pitcavage et al., 2021). Involvement of mantle peridotite in the melting process would cause a dilution of the melt, resulting in less extreme composition (e.g. lower alkali contents). The type of interaction is strongly affected by the Mg# of the melt and the eventual equilibrium condition with the surrounding mantle (e.g. Foley et al. 2025).

TA melts produced at 2.7 GPa and 1350-1400 °C (60 and 90 wt.% melt, respectively) show good overlap with natural kamafugites for almost all the oxides (e.g.  $SiO_2$ ,  $Al_2O_3$ , MgO,  $K_2O$  and  $P_2O_5$ ).  $TiO_2$  and CaO differ only slightly, with higher contents in the synthetic glasses than for the natural rocks (see Innocenzi et al. 2024a and references therein).  $Na_2O$  (0.39-0.78 wt.%) is displaced toward the lower end of the field of natural samples (0.18-3.60 wt.%; Innocenzi et al. 2024a and reference therein; Fig. 7). At 5 GPa, experimental melts at 1450, 1500 and 1550 °C (64, 72 and 85 wt.% melt, respectively; Fig. 1) approach natural compositions.  $SiO_2$ ,  $Al_2O_3$ , MgO and  $K_2O$  match well, whereas CaO,  $Na_2O$ , and  $P_2O_5$  only partially overlap (Fig. 8).  $TiO_2$  contents in all analysed glasses is too high,

and only at 1550 °C there is an overlap with the upper end of the natural kamafugite field (5.1-5.3 wt.% in synthetic glass vs. 3.0-6.1 wt.% in natural Ugandan samples).

Brazilian kamafugites, from both the APIP and Goiás Alkaline Provinces (GAP, SE Brazil) are plotted together to give a better representation of compositions of the whole region and to allow a better comparison with other natural kamafugites. As for the other two cases, the differences among the different Brazilian kamafugites can be partially ascribed to the effects of diffuse alteration events, such as analcimization (e.g. Sgarbi and Gaspar, 2002; Brod et al. 2005; Melluso et al. 2008; Guarino et al. 2013). APIP experimental glass obtained at 2.7 GPa and 1350 to 1400 °C (50 and 70 wt.% melt, respectively) show good overlap with natural kamafugites for almost all the major oxides (e.g. SiO<sub>2</sub>, Al<sub>2</sub>O<sub>3</sub>, MgO, K<sub>2</sub>O and P<sub>2</sub>O<sub>5</sub>). TiO<sub>2</sub> and CaO only slightly differ, with higher values in the synthetic glasses than for the natural rocks (Innocenzi et al. 2025 and references therein). Na<sub>2</sub>O (0.38-0.81 wt.%) is displaced toward the lower end of the field of natural samples (0.05-4.45 wt.%; Innocenzi et al. 2025 and reference therein; Fig. 7).

As regards IAP, only literature data from San Venanzo and Cupaello lavas with SiO<sub>2</sub> higher than 38.1 wt.% are reported, as this province also hosts many pyroclastic products containing variable amounts of secondary carbonate-bearing lithologies (Lustrino et al. 2019; 2020; 2025; Innocenzi et al. 2024b and reference therein). Despite being spatially and temporally very close, the eruptive centres of San Venanzo and Cupaello are characterized by distinct geochemical (i.e. San Venanzo kamafugites have lower TiO<sub>2</sub> and higher MgO-Al<sub>2</sub>O<sub>3</sub> than Cupaello) and mineral paragenesis (e.g. San Venanzo lavas are olivine-rich clinopyroxene-poor, whereas Cupaello lavas are almost completely olivine-free and clinopyroxene-rich; Lustrino et al. 2020; 2025). Recently, Lustrino et al. (2025) attributed these differences to a prolonged fractional crystallization history (olivine + phlogopite + melilite + spinel + kalsilite) starting from a less evolved magma similar in composition to San Venanzo primitive kamafugite (sample SAV6 of Lustrino et al. 2020). Despite the non-primitive composition, Innocenzi et al. (2024c) performed near-liquidus experiments on a Cupaello sample in order to evaluate other possibilities. It is plausible that the lithospheric mantle beneath central Italy could be extremely heterogeneous and laterally variable, involving slightly different metasomatic assemblages (i.e. variable concentrations of metasomatic phlogopite and clinopyroxene). This, coupled with different degrees of partial melting could be an alternative explanation of the several differences between San Venanzo and Cupaello. As the matter is still debated, both San Venanzo and Cupaello data are reported on the Harker diagrams (Figs 7 and 8), thus resulting in the wide field of IAP kamafugites.

Only the 2.7 GPa experiments carried out at 1350 and 1400 °C partially overlap the natural IAP rocks. The most remarkable difference occurs for TiO<sub>2</sub>, which is very low in San Venanzo and

Cupaello volcanic rocks (<1.3 wt.%), compared to the experimental glasses (>3.8 wt.%). MgO shows slightly lower values (6.4-12.5 wt.%) in the experimental melts than in the natural San Venanzo samples (7.6-15.5 wt.%; Appendix 1).  $P_2O_5$  in the IAP experimental glasses are too high (1.3-1.4 wt.%) with respect to the natural San Venanzo composition (0.32-1.44 wt.%), whereas they overlap for the Cupaello samples (~1.2 wt.%). These characteristics for Cupaello may be interpreted as a primary feature of the mantle source, but they may also result from the fractionation of an apatite-free kalsilitolite cumulate, to allow for the increase of  $P_2O_5$  in the residual melt (e.g. Lustrino et al. 2025). A fractionation history for Cupaello lavas is also supported by the poor overlap of IAP experimental glasses with the natural rocks, with the exception of  $SiO_2$ ,  $Al_2O_3$  and  $P_2O_5$  at 1400 °C.

At 5 GPa, experimental glasses for IAP and TA at 1450, 1500 and 1550 °C (80 to 90 wt.% melt; Fig. 1) approach the natural compositions. For IAP, the agreement is weaker than for TA, as most major oxides do not fall in the natural rock fields (e.g. higher  $TiO_2$ , lower  $Al_2O_3$  and CaO). This may be caused by the high degree of partial melting, which would dilute  $Al_2O_3$  and  $K_2O$ , whose values are lower than the natural examples, causing an increase in MgO and CaO from the clinopyroxene, which is the last mineral phase to completely melt out. For IAP, at 1400 °C (~40 wt.% melt) the overlap with natural compositions improves for MgO and  $K_2O$ , but the experimental melt composition is still strongly influenced by the undiluted contribution from the accessory phases. Also the crystallization of tschermakite would affect the composition of the resulting glasses. A degree of partial melting between 40 and 80 wt.% could likely shift the compositions of melts towards natural compositions.

## 5.2 Further consideration on source parageneses

Past melting experiments on hydrous mineral-rich non-peridotitic ultramafic compositions (such as phlogopite-bearing clinopyroxenites) show solidi consistently lower than peridotite, even when compared with hydrous peridotite compositions (e.g. Kogiso et al., 2004; Lambart et al., 2012; Ezad et al. 2024; Foley et al., 2025). The composition of hydrous non-peridotitic ultramafic rocks is sensitive to the modal abundances of phases entering the melt, both as concerns major oxides (Foley et al. 2022) and trace elements (Foley and Ezad, 2024). The differences between natural kamafugites and the experimental glasses reported in this study may thus be related to different modal proportions of the minerals in the mantle sources and/or on the variable compositions of each phase.

The experimental melts are always characterised by higher  $TiO_2$  than natural kamafugites. For TA and APIP, this is probably due to the phlogopite used in the experiments, which likely has a higher  $TiO_2$  content than the phlogopite in the source of these two regions. Alternatively, it may be explained by a lower amount of titanite and/or ilmenite (~1-2%) in the melting assemblage. For IAP,

this may be caused either by an excessive  $TiO_2$  content of clinopyroxene (1.58 wt.%) or by a too high proportion of magnetite (9.40 wt.%) in the starting material. Alternatively, considering the subduction-modified composition of IAP rocks (e.g. Lustrino et al. 2011; 2022), the low  $TiO_2$  content could simply be a mantle source characteristic.

The other main differences are in Na<sub>2</sub>O and in K<sub>2</sub>O/Na<sub>2</sub>O ratio, which tend to be respectively higher and lower in the natural rocks than in the experimental melts, especially those at 2.7 GPa (Figs. 7 and 8). This issue related to Na<sub>2</sub>O has previously been recognised for TA kamafugites (e.g. Lloyd et al. 1985) but remains unsolved. It is unlikely to be related to the presence of amphibole in the melting assemblage. Indeed, near-liquidus experiments (e.g. Edgar et al. 1976; Innocenzi et al. 2024c) seem to exclude the stability of amphibole in kamafugite mantle sources, and no amphibole has been found in the abundant nodules embedded in the Ugandan kamafugites (e.g. Link et al. 2008). In a set of partial melting experiments on phlogopite-bearing clinopyroxenite nodules, Lloyd et al. (1985) used a clinopyroxene with higher Na<sub>2</sub>O (about 1.15 wt.%) than the one used in this study (0.51 wt.%), obtaining, glass with higher Na<sub>2</sub>O (up to 1.95 wt.%). This is much more coherent with the TA natural composition, which hosts clinopyroxenes with 0.18-2.61 wt.% Na<sub>2</sub>O. Finally, less than 1% of apatite in TA melting assemblage would guarantee a good match between natural and experimental compositions.

For APIP, the difference in  $Na_2O$  content is even higher. Experiments conducted at near-liquidus conditions (1350 °C; 2 GPa) and at lower temperature (1000 °C; 2 GPa; Innocenzi et al. 2024c) resulted in crystallization of clinopyroxene with a  $Na_2O$  content ranging from 0.72 (sub-liquidus run) to 2.05 wt.% (near-liquidus run). The much lower  $Na_2O$  content of the clinopyroxene used in this study (0.51 wt.%) can easily account for the divergence between the experimental glasses and the natural samples. Guarino et al. (2024) analysed diopsidic clinopyroxene from xenocrysts and lherzolite xenoliths in APIP kimberlites with  $Na_2O$  in the 1.02-1.72 wt.% range. It follows that relatively  $Na_2O$ -rich clinopyroxene can be present in APIP lithospheric mantle, but unfortunately, mineralogical constraints for the APIP kamafugite mantle source from natural rocks are more restricted than for TA.

The good match with MgO between natural TA kamafugites and experimental glasses may support the hypothesis that no olivine is involved in the genesis of Ugandan kamafugites (Appendix 1). Indeed, olivine is not needed to explain the geochemical features of the lavas, and the nodules almost completely lack this phase (Link et al. 2008; Innocenzi et al. 2022; 2024a). The lower melting temperature of the metasomatic veins than surrounding peridotite, coupled with the high mobility of the melts would have caused a rapid upwelling to the surface limiting interaction with the surrounding peridotite mantle (Foley et al. 1999; Foley and Ezad; 2024). Interestingly, the MgO

content of APIP experimental glasses (10.3-16.5 wt.%), where olivine was included in the starting materials, are very similar to that recorded for TA (10.6-16.0 wt.%) at the same conditions, where no olivine was used in the starting material. This is probably because olivine gives little contribution to the melt at low melting degrees. In order to obtain higher MgO content in the experimental glass, even higher melting degrees should be reached.

The IAP experimental glasses display lower MgO content than Italian kamafugites, possibly due to the peritectic crystallization of olivine formed through incongruent melting of phlogopite, which would decrease MgO in the glass (e.g. Prelević et al., 2024; Foley et al., 2025). Alternatively, we can interpret the lower MgO in the IAP experimental glasses to the actual presence of olivine in San Venanzo mantle source, which was not used in the starting material of experiments. The presence of low amounts of highly magnesian olivine participating to the melts may result in a better overlap with the natural melt compositions. It is also important to highlight that previous literature studies (e.g. Lustrino et al. 2020) suggested a limited digestion of country rocks (mainly carbonates) by an ultrabasic magma in San Venanzo, a process that could have contributed to the discrepancy observed between natural and synthetic compositions. The melting assemblage in San Venanzo must also have contained <1 wt.% of apatite to ensure a better overlap between natural and experimental values, as supposed for the TA case.

The presence of olivine in the melting assemblages suggested for APIP and IAP may be related to the reaction with the surrounding mantle, either after the partial melting of the hydrous metasomes or during the percolation of the metasomatic fluids (Foley et al. 1992; Mallik et al., 2021; Shu et al. 2024; Innocenzi et al. 2024c; Prelević et al., 2024). Another crucial point could be represented by the composition of the surrounding mantle, i.e. ultra-depleted or fertile assemblages, which reacts differently with the percolating melts/liquids (e.g. Cooper et al. 2024).

# **6 Conclusions**

Partial melting experiments have been carried out on assemblages spanning from phlogopite clinopyroxenite ( $\pm$  olivine) to clinopyroxene glimmerite at 1250-1550 °C and a 2.7-5 GPa. The produced glasses are characterised by extremely variable compositions, strongly influenced by the degree of melting and by the relative contributions of the mineral phases to the melt. Relatively low-degree partial melting results in extreme compositions (e.g. very low SiO<sub>2</sub>, very high high TiO<sub>2</sub> and P<sub>2</sub>O<sub>5</sub>), due to the participation of titanite, apatite and Fe-Ti-oxides in TA, apatite and ilmenite in APIP, and apatite and magnetite in IAP in the melting assemblage. In these cases, the experimental glasses do not mimic any natural silicate igneous rocks, but they probably represent good candidates for metasomatic melts infiltrating within the lithospheric mantle matrix (Fitzpayne et al., 2019; Foley et al. 2022). Metasomatic products in mantle xenoliths commonly contain high proportions of Ti- and

Fe-Oxide minerals (Harte et al., 1987). The volatile-rich nature of these melts will also affect their physical and chemical properties resulting in lower density and higher mobility compared to anhydrous  $SiO_2$ -rich compositions (Russell et al., 2022; Schäfer and Foley, 2002; Prelević et al., 2024). With increasing temperature and amount of melt produced, glass compositions approach those of natural magmas, whose main characteristics are low silica, high alkali (especially  $K_2O$ ) and high lime. The results of partial melting experiments suggest that high degrees of partial melting (>50 wt.%) of clinopyroxene  $\pm$  phlogopite assemblages found in the lithospheric mantle can lead to the formation of ultrapotassic and/or ultracalcic compositions. This confirms the hypothesis of Lloyd et al. (1985), according to which the Toro Ankole ultrapotassic rocks could be derived from hydrous ultramafic sources.

We observe a partial overlap between the compositions of experimental glasses and natural kamafugites. In particular, a good match for some major oxides (especially SiO<sub>2</sub>, MgO, K<sub>2</sub>O and P<sub>2</sub>O<sub>5</sub>) with experiments at 1350 and 1400 °C is observed for Brazilian and Ugandan lavas. This could illustrate the importance of clinopyroxene as dominant phase (50 and 60 wt.% for Brazilian and Ugandan lavas, respectively) contributing to melt composition, coupled with phlogopite and other accessory phases, such as apatite and ilmenite. As the modal abundance of phlogopite in the starting materials of the TA experiments was higher than for APIP, the K<sub>2</sub>O content of the experimental glass was consequently higher, together with Al<sub>2</sub>O<sub>3</sub>. Experimental results also support the presence of olivine in the APIP source, even if only partially contributing to the MgO budget. On the other hand, the composition of the experimental glasses produced from an olivine-free phlogopite-pyroxenite assemblage, are in reasonable agreement with those of the natural kamafugites from the Toro Ankole volcanic Province.

The experimental glasses obtained from the clinopyroxene glimmerite assemblage roughly match the lava compositions from San Venanzo, with the suggestion of the presence of olivine in the melting assemblage in addition to a slightly lower amount of magnetite and apatite. Experimental results confirm the importance of phlogopite in the source of Italian kamafugites, contributing to their very high  $K_2O$  content, and of clinopyroxene, responsible for the high CaO content. The possible interaction between San Venanzo magmas and sedimentary limestones (Lustrino et al., 2020) may further complicate the Italian framework, as well as the presence of carbonates in the sources, a feature not investigated in the present study.

The presence of accessory phases in the mineral assemblage of mantle sources is fundamental to explain many of the geochemical features of the natural rock samples. For example, apatite (<3 wt.%) controls the  $P_2O_5$  content of the whole-rock, whereas titanite (<4 wt.%) and ilmenite (<5 wt.%) are required to reach the high  $TiO_2$  content of the Ugandan and Brazilian kamafugites (3.0-9.5 wt.%).

This indicates that the large spectrum of compositions of the natural lavas may be related to different degrees of melting of clinopyroxenite (± olivine) variably enriched in phlogopite and some accessory minerals, such as apatite and TiO<sub>2</sub>-bearing phases. Different abundances of the main (clinopyroxene and phlogopite) and accessory (e.g. olivine) phases in the mantle sources are probably related to laterally heterogeneous lithospheric mantles. This, together with variable degree of melting and interaction with the surrounding peridotitic matrix, with or without additional crustal interaction at shallow depth, would be able to give rise to almost all the primitive kamafugite magma compositions.

#### 7 Acknowledgements

The present work is a distillation of the PhD thesis of the first author at Sapienza University of Rome. It was financially supported by funds Ateneo Sapienza 2022 and 2024 to ML, Ateneo Sapienza 2022 to SR and Ateneo Sapienza 2023 to Silvio Mollo, by IGG–CNR P-CT0049 to SA, by "Avvio alla Ricerca" grant 2022 to FI and by Australian Research Council grant FL180100134 to SFF.

The authors thank Domenico Mannetta for his help during the polishing process. FI thanks Dr. Sean Murray for his help in the Macquarie GeoAnalytical Laboratories. FI also thanks professors Lorenzo Fedele (University of Naples Federico II, Italy) and Michele Mattioli (University of Urbino Carlo Bo, Italy) for their help in improving the readability of an early version of this manuscript in the form of PhD thesis manuscript.

#### 8 Declaration of interests

The authors declare that they have no known competing financial interests or personal relationships that could have appeared to influence the work reported in this paper.

#### 9 References

Bohlen S. and Boettcher A.L. (1982) The quartz coesite transformation: A precise determination and the effect of other components. *Journal of Geophysical Research*, **87**, 7073-7078.

Borghini G., Fumagalli P. and Rampone E. (2017) Partial melting of secondary pyroxenite at 1 and 1.5 GPa, and its role in upwelling heterogeneous mantle. *Contributions to Mineralogy and Petrology*, **172**, 70.

Brod J.A., Barbosa E.S.R., Junqueira-Brod T.C., Gaspar J.C., Diniz-Pinto H.S., Sgarbi P.B.A. and Petrinovic I.A. (2005) The Late-Cretaceous Goiás Alkaline Province (GAP), Central Brazil. Pp. 261-340 in: *Mesozoic to Cenozoic Alkaline Magmatism in the Brazilian Platform* (P. Comin-Chiaramonti and C.B. Gomes, editors). Editora de Universidade de São Paulo, São Paulo.

Cooper N.P., Scott J.M., Brenna M., Palmer M.C., le Roux P.J., Cooper A.F., Reid M.R. and Stirling, C.H. (2024) Hydrous veined mantle lithosphere and implications for the source of Zealandia intraplate magmas. *Lithos*, **478**, 107608.

Eby, G.N., Lloyd, F.E., Woolley, A.R. (2009) Geochemistry and petrogenesis of the Fort portal, Uganda, extrusive carbonatite. *Lithos* **113**, 785-800.

- Edgar, A.D., Green, D.H., Hibberson, W.O. (1976). Experimental petrology of a highly potassic magma. Journal of Petrology, 17, 339-356.
- Ezad I.S., Shcheka S.S., Buhre S., Buhre A., Gorojovsky L.R., Shea J.J., Förster M.W. and Foley S.F. (2023) Rapid quench piston cylinder apparatus: An improved design for the recovery of volatile-rich geological glasses from experiments at 0.5–2.5 GPa. *Review of Scientific Instruments*, **94**, 055107.
- Ezad I.S., Blanks D.E., Foley S.F., Holwell D.A., Bennett J. and Fiorentini M.L. (2024) Lithospheric hydrous pyroxenites control localitation and Ni endowment of magmatic sulfide deposits. *Mineralium Deposita*, **59**, 227-236.
- Foley S.F. (1992) Petrological characterization of the source components of potassic magmas: geochemical and experimental constraints. *Lithos*, **28**, 187-20.
- Foley S.F., Musselwhite D.S. and van der Laan S.R. (1999) Melt Compositions from Ultramafic Vein Assemblages in the Lithospheric Mantle: A Comparison of Cratonic and Non-Cratonic Settings. 7th International Kimberlite Conference, April 1988.
- Foley S.F. (2008) Rejuvenation and erosion of the cratonic lithosphere. *Nature Geoscience*, **1**, 503-510. Foley S.F. and Ezad I.S. (2024) Melting of hydrous pyroxenites with alkali amphiboles in the continental mantle: 2. Trace element compositions of melts and minerals. *Geoscience Frontiers*, **15**, 101692.
- Foley S.F., Ezad I.S., van der Laan S.R. and Pertermann M. (2022). Melting of hydrous pyroxenites with alkali amphiboles in the continental mantle: 1. Melting relations and major element compositions of melts. *Geoscience Frontiers*, **13**, 101380.
- Foley S.F., Ezad I.S., Shu C., Förster M.W. (2025) Melting of amphibole-apatite-rich metasomes in the continental mantle and comparison of melt compositions with natural igneous rocks. *Lithos*, **500**-**501**, 107976.
- Förster M.W., Prelević D., Schmück H.R., Buhre S., Veter M., Mertz-Kraus R., Foley S.F. and Jacob D.E. (2017) Melting and dynamic metasomatism of mixed harzburgite + glimmerite mantle source: implications for the origin of orogenic potassic magmas. *Chemical Geology*, **455**, 182–191.
- Förster M.W., Buhre S., Xu B., Prelević D., Mertz-Kraus R. and Foley S.F. (2019) Two-stage origin of K-enrichment in ultrapotassic magmatism simulated by melting of experimentally metasomatized mantle. *Minerals*, **10**, 41.
- Frey F.A., Green D.H. and Roy S.D. (1978) Integrated models of basalt petrogenesis: a study of quartz tholeiites to olivine melilitites from south eastern Australia utilizing geochemical and experimental petrological data. *Journal of Petrology*, **19**, 463-513.
- Funk S. P. and Luth R. W. (2013) Melting phase relations of a mica–clinopyroxenite from the Milk River area, southern Alberta, Canada. *Contributions to Mineralogy and Petrology*, **166**, 393-409.
- Green D.H. (1970) The origin of basaltic and nephelinitic magmas. *Transactions of the Leicester Philosophical and Literary Society*, **64**, 28-54.
- Guarino V., Wu F.Y., Lustrino M., Melluso L., Brotzu P., de Barros Gomes C., Ruberti E., Tassinari C.C.G. and Svisero D.P. (2013). U-Pb ages, Sr–Nd-isotope geochemistry, and petrogenesis of kimberlites, kamafugites and phlogopite-picrites of the Alto Paranaíba Igneous Province, Brazil. *Chemical Geology*, **353**, 65-82.
- Guarino V., Bonazzi M., Nimis P., Azzone R. G., Cariddi B. and Zanetti A. (2024) Stabilization and evolution of the Brazilian subcontinental lithospheric mantle: Insights from garnet xenocrysts and peridotite xenoliths of Três Ranchos kimberlite (APIP, Brazil). *Gondwana Research*, **130**, 18-35.
- Harte, B., Winterbrun, P.A., Gurney, J.J. (1987) Metasomatic and enrichment phenomena in garnet peridotite facies mantle xenoliths from the Matsoku kimberlite pipe, Lesotho. In: (Menzies, M.A., Hawkesworth, C.J., Eds.) *Mantle Metasomatism*, Academic Press, London, U.K., pp.145-220.

- Holland T.J. (1980) The reaction albite = jadeite + quartz determined experimentally in the range 600-1200 °C. *American Mineralogist*, **65**, 129-134.
- Innocenzi F., Ronca S., Foley S.F., Agostini S. and Lustrino M. (2022) Exotic magmatism from the western branch of the East African Rift: insights on the lithospheric mantle source. EGU General Assembly, Vienna, Austria, May 2022.
- Innocenzi F., Ronca S., Agostini S., Guarino V., Foley S. F., Lustrino M. (2025) Kamafugites. Earth-Science Reviews, 105238.
- Innocenzi F., Ronca S., Foley S. F., Agostini S. and Lustrino M. (2024a) Carbonatite and ultrabasic magmatism at Toro Ankole and Virunga, western branch of the East African Rift system. *Gondwana Research*, **125**, 317-342.
- Innocenzi F., Ronca S., Agostini S., Benedetti F. and Lustrino M. (2024b) On the occurrence of kalsilite in melilite-bearing ultrapotassic lavas from the Roman Province (Vulsini Mts., central Italy). *Lithos*, **482-483**, 107704.
- Innocenzi F., Ezad I.S., Ronca S., Agostini S., Lustrino M. and Foley S.F. (2024c) Experimental petrology constraints on kamafugitic magmas. *European Journal of Mineralogy*, **36**, 899-916.
- Keshav S., Gudfinnsson G.H., Sen G. and Fei Y. (2004) High-pressure melting experiments on garnet clinopyroxenite and the alkalic to tholeiltic transition in ocean-island basalts. *Earth and Planetary Science Letters*, **223**, 365-379.
- Kiseeva E.S., Kamenetsky V.S., Yaxley G.M. and Shee S.R. (2017) Mantle melting versus mantle metasomatism—"The chicken or the egg" dilemma. *Chemical Geology*, **455**, 120-130.
- Klemme S., Blundy D.J. and Wood B.J. (2002) Experimental constraints on major and trace element partitioning during partial melting of eclogite. *Geochimica et Cosmochimica Acta*, **66**, 3109-3123.
- Kogiso T. and Hirschmann M.M. (2001) Experimental study of clinopyroxenite partial melting and the origin of ultra-calcic melt inclusions. *Contributions to Mineralogy and Petrology*, **142**, 347-360.
- Kogiso T., Hirschmann M.M. and Pertermann M. (2004) High-pressure partial melting of mafic lithologies in the mantle. *Journal of Petrology*, **45**, 2407–2422.
- Konzett J. (1997) Phase relations and chemistry of Ti-rich K-richterite-bearing mantle assemblages: an experimental study to 8 GPa in a Ti-KNCMASH system. *Contributions to Mineralogy and Petrology,* 128 385-404
- Konzett J., Sweeney R.J., Thomposon A.B. and Ulmer P. (1997) Potassium amphibole stability in the upper mantle: an experimental study in a peralkaline KNCMASH system to 8.5 GPa. *Journal of Petrology*, **38**, 537-568.
- Lambart S., Laporte D., Provost A. and Schiano P. (2012). Fate of pyroxenite-derived melts in the peridotitic mantle: thermodynamic and experimental constraints. *Journal of petrology*, *53*, 451-476.
- Le Maitre R.W. (2002) Classification of igneous rocks and glossary of terms. Recommendations of the *IUGS Subcommission on the Systematics of Igneous Rocks*. Cambridge University Press, Cambridge, 254 pp.
- Link K., Barifaijo E., Tiberindwa J. and Foley S.F. (2008). Veined pyroxenite xenoliths from the kamafugites in the Toro Ankole region of western Uganda: a window to a rift-related mantle. 9<sup>th</sup> International Kimberlite Conference, August 2008.
- Lloyd F.E., Arima M. and Edgar A.D. (1985) Partial melting of a phlogopite-clinopyroxenite nodule from south-west Uganda: an experimental study bearing on the origin of highly potassic continental rift volcanics. *Contributions to Mineralogy and Petrology*, **91**, 321-329.
- Lustrino M., Chiarabba C. and Carminati E. (2022) Igneous activity in central-southern Italy: is the subduction paradigm still valid? Pp. 1–16 in: *In the Footsteps of Warren B. Hamilton: New ideas in*

- *Earth Science* (G.R. Foulger, L.C. Hamilton, D.M. Jurdy, C.A. Stein, K.A. Howard, and S. Stein, editors). Geological Society of America Special Paper, 553, Boulder, Colorado.
- Lustrino M., Duggen S. and Rosenberg C.L. (2011). The Central-Western Mediterranean: anomalous igneous activity in an anomalous collisional tectonic setting. *Earth-Science Reviews*, **104**, 1-40.
- Lustrino M., Luciani N. and Stagno V. (2019). Fuzzy petrology in the origin of carbonatitic/pseudocarbonatitic Ca-rich ultrabasic magma at Polino (central Italy). *Scientific Reports*, **9**, 9212.
- Lustrino M., Ronca S., Caracausi A., Ventura Bordenca C., Agostini S. and Faraone D.B. (2020). Strongly SiO<sub>2</sub>-undersaturated, CaO-rich kamafugitic Pleistocene magmatism in Central Italy (San Venanzo volcanic complex) and the role of shallow depth limestone assimilation. *Earth-Science Reviews*, **208**, 103256.
- Lustrino M., Pistocchi L., Ronca S., Innocenzi F. and Agostini S. (2022) Carbonate assimilation of ultrabasic magma: the Pleistocene Cupaello kamafugitic volcano (central Italy). EGU General Assembly, Vienna, Austria, 23-27 May 2022.
- Lustrino M., Pistocchi L., Ronca S., Innocenzi F. and Agostini S. (2025) Origin of ultrapotassic, ultracalcic, ultrabasic SiO<sub>2</sub>-undersaturated magmas. The case study of the Pleistocene Cupaello kamafugite monogenetic volcano, central Italy. *Geochemistry Geophysics Geosystems*, **26**, 1, e2024GC011683.
- Mallik A., Lambart S. and Chin E. J. (2021). Tracking the evolution of magmas from heterogeneous mantle sources to eruption. *Mantle convection and surface expressions*, 151-177.
- Melluso L., Lustrino M., Ruberti E., Brotzu P., De Barros Gomes C., Morbidelli L., Morra V., Svisero D.P. and d'Amelio F. (2008) Major and trace-element compositions of olivine, perovskite, clinopyroxene, Cr-Fe-Ti oxides, phlogopite and host kamafugites and kimberlites, Alto Paranaiba, Brazil. *Canadian Mineralogist*, **46**, 19-40.
- Mjelde R., Wessel P. and Müller R.D. (2010) Global pulsations of intraplate magmatism through the Cenozoic. *Lithosphere*, **2**, 361-376.
- Muravyeva N.S., Belyatsky B.V., Senis V.G. and Ivanov A.V. (2014) Sr-Nd—Pb isotope systematics and clinopyroxene-host disequilibrium in ultra-potassic magmas from Toro Ankole and Virunga, East-African Rift: Implications for magma mixing and source heterogeneity. *Lithos*, **210-211**, 260-277.
- Pitcavage E., Furman T., Nelson W. R., Kalegga P. K. and Barifaijo E. (2021). Petrogenesis of primitive lavas from the Toro Ankole and Virunga Volcanic Provinces: metasomatic mineralogy beneath East Africa's Western rift. *Lithos*, *396*, 106192.
- Prelević D., Förster M. W., Buhre S., Gülmez F., Grützner T., Wang Y., and Foley S. F. (2024). Recent advances made by reaction experiments on melting of heavily metasomatized hydrous mantle. *Earth-Science Reviews*, 104881
- Roden M.F. and Murthy V.R. (1985) Mantle metasomatism. *Annual Review of Earth and Planetary Sciences*, **13**, 269-296.
- Rosenthal A., Foley S.F., Pearson D.G., Nowell G.M. and Tappe S. (2009) Petrogenesis of strongly alkaline primitive volcanic rocks at the propagating tip of the western branch of the East African Rift. *Earth and Planetary Science Letters*, **284**, 236-248.
- Russell J.K., Hess K.U. and Dingwell D.B. (2022) Models for viscosity of geological melts. *Reviews in Mineralogy and Geochemistry*, **87**, 841-885.
- Schafer, F.N., Foley, S.F., 2002. The effect of crystal orientation on the wetting behaviour of silicate melts on the surfaces of peridotite minerals. *Contribution to Mineralogy and Petrology*, **143**, 254–262.

- Sgarbi P.B.A. and Gaspar J.C. (2002) Geochemistry of Santo Antônio da Barra Kamafugites, Goiás, Brazil. *Journal of South American Earth Sciences*, **14**, 889-901.
- Shu C.T., Foley S.F., Ezad I.S., Daczko N.R. and Shcheka S.S. (2024) Experimental melting of phlogopite websterite in the upper mantle between 1.5 and 4.5 GPa. *Journal of Petrology*, **65**, egae030.
- Spandler C., Yaxley G.M., Green D.H. and Rosenthal A. (2008) Phase relations and melting of anhydrous K-bearing eclogite from 1200 to 1600°C and 3 to 5 GPa. *Journal of Petrology*, **49**, 771-795.
- Sweeney R.J., Thompson A.B. and Ulmer P. (1993) Phase relations of a natural MARID composition and implications for MARID genesis, lithospheric melting and mantle metasomatism. Contributions to Mineralogy and Petrology, **115**, 225-241.
- Tappe S., Foley S.F. and Pearson D.G. (2003) The kamafugites of Uganda: a mineralogical and geochemical comparison with their Italian and Brazilian analogues. *Periodico di Mineralogia*, **72**, 51-77.
- Yaxley G.M. and Green D.H. (1998) Reactions between eclogite and peridotite: mantle refertilisation by subduction of oceanic crust. *Schweizerische mineralogische und petrographische Mitteilungen*, **78**, 243-255.
- Zartner S. (2010) Charakterisierung und Entstehung kamafugitischer und karbonatitischer lapillituffe aus Toro-Ankole, Uganda. Master thesis, Johannes Gutenberg-Universität Mainz, Germany.
- Zhang J., Li B., Utsumi W. and Liebermann R.C. (1996) In situ X-ray observations of the coesite-stishovite transition: reversed phase boundary and kinetics. *Physics and Chemistry of Minerals*, **23**, 1-10.

# **10 Figure Captions**

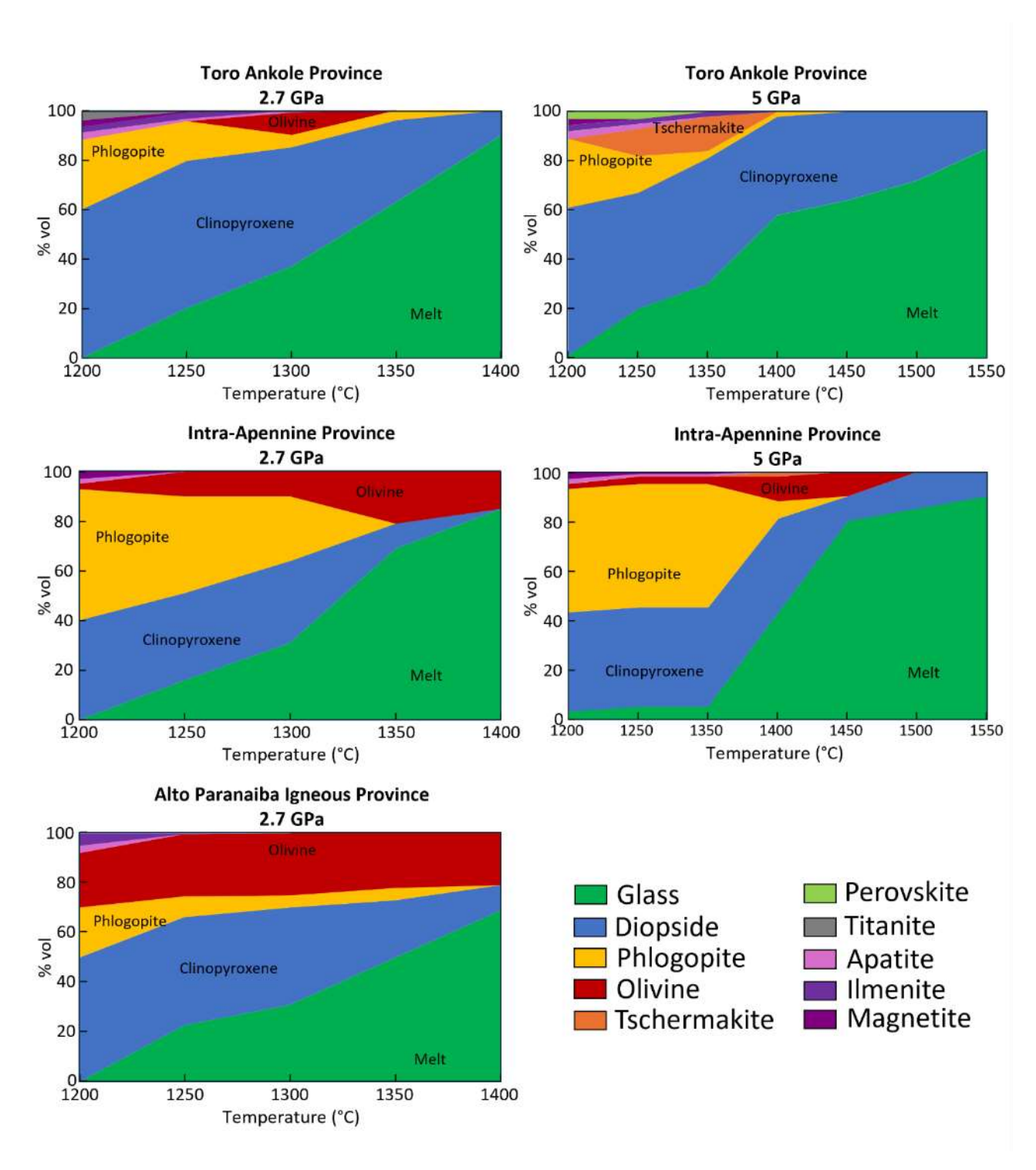


Fig 1. Modal abundances (wt.%) of mineral phases and melt (glass) obtained in each experimental samples (TA, IAP and APIP) at 2.7 and 5 GPa.

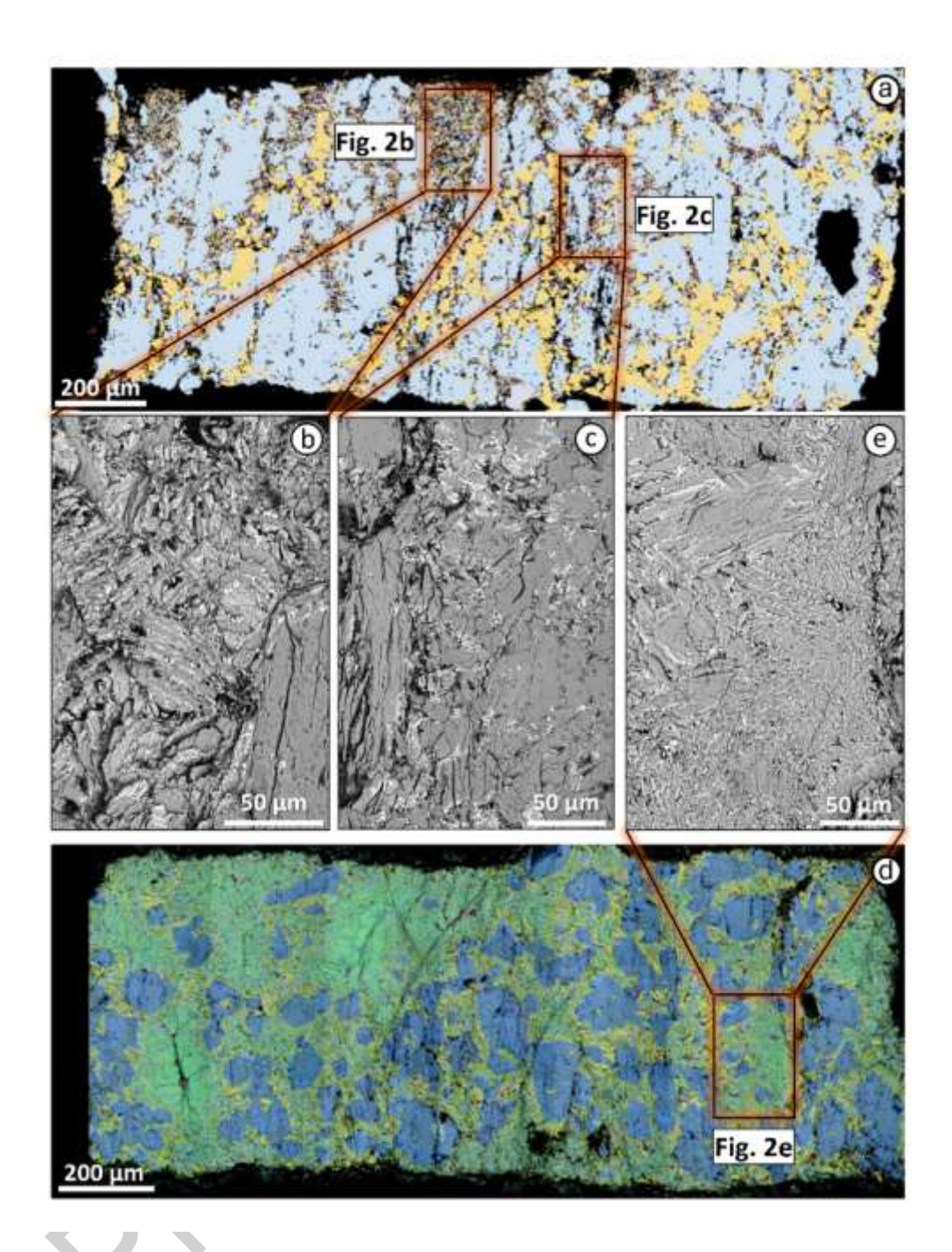


Fig. 2. (a) Field-emission-scanning electron microscopy (FESEM) mineral maps on TA experimental sample A23-012 (2.7 GPa and 1250 °C); (b) and (c) higher magnification SEM microphotographs of quenched needles. (d) FESEM mineral maps on TA experimental sample A23-016 (2.7 GPa and 1350 °C); (e) higher magnification SEM microphotographs of melt pools. Dark blue stands for clinopyroxene, light blue for augite, orange for tschermakite, yellow for phlogopite, red for olivine, purple for ilmenite, pink for apatite, light green for perovskite and green for glass.

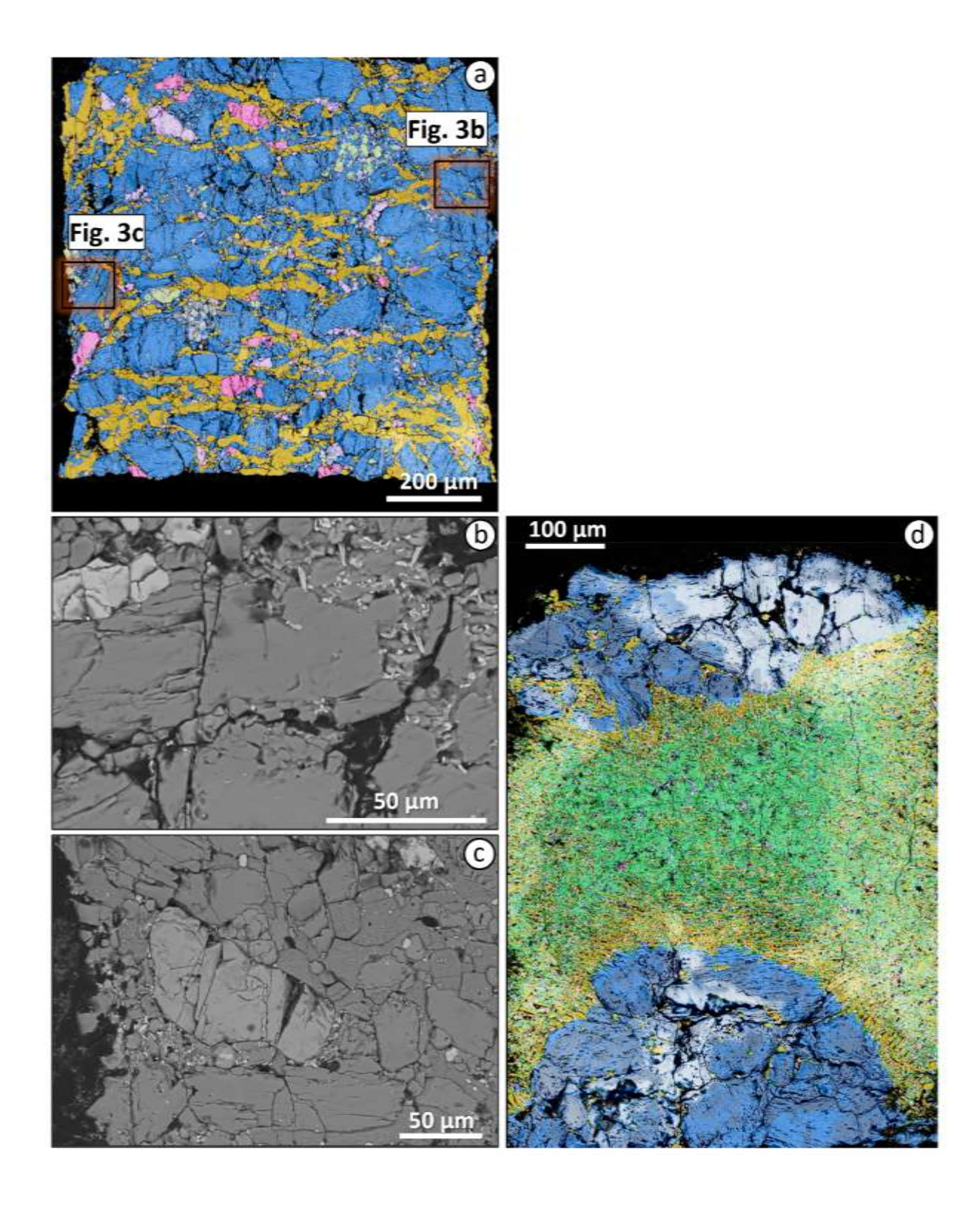


Fig. 3. (a) FESEM mineral maps on TA experimental sample M22-005 (5 GPa and 1200  $^{\circ}$ C); (b) and (c) higher magnification SEM microphotographs of quenched needles. (d) FESEM mineral maps on TA experimental sample M22-010 (5 GPa and 1400  $^{\circ}$ C). Colours as in Fig. 2.

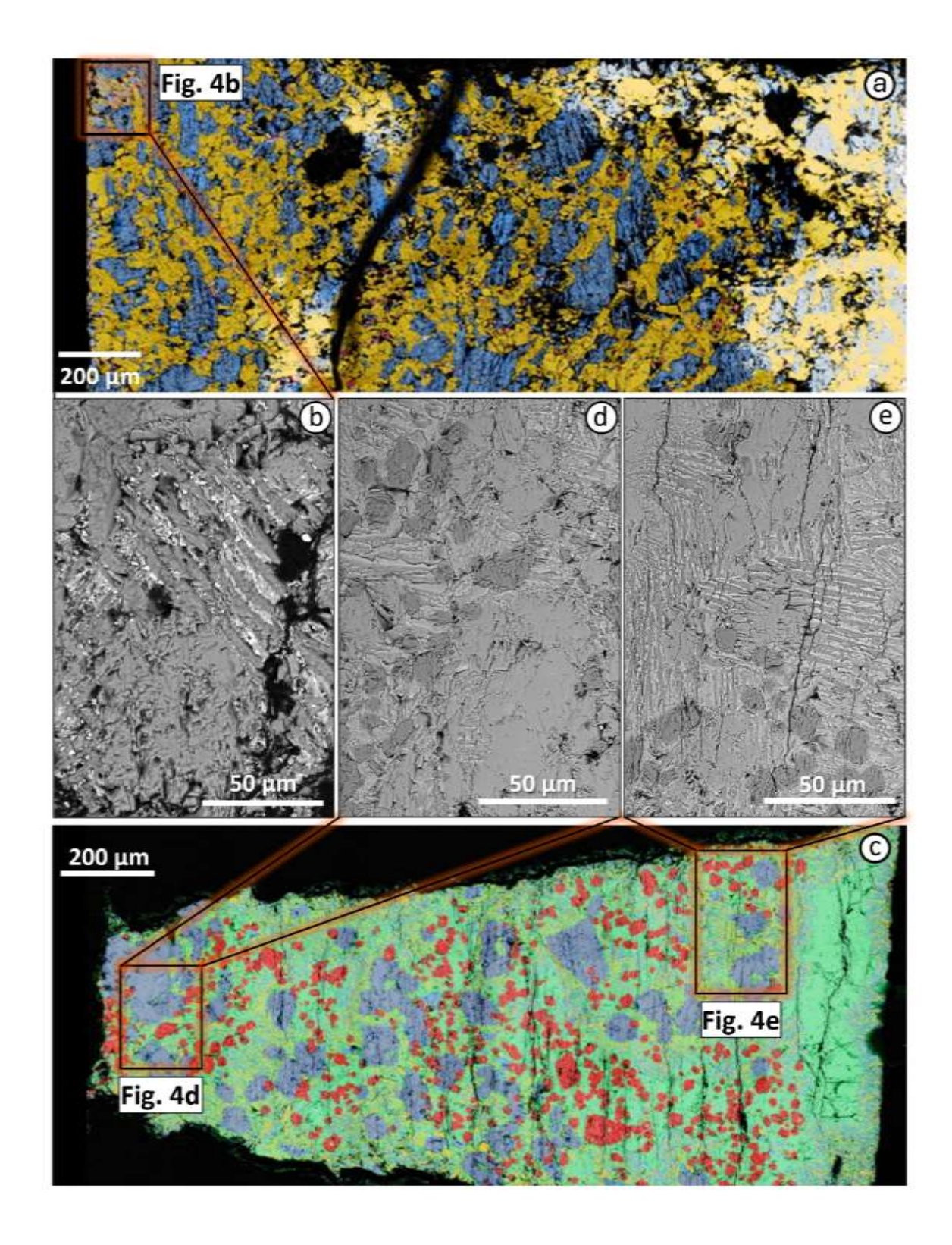


Fig. 4. (a) FESEM mineral maps on IAP experimental sample A23-012 (2.7 GPa and 1250 °C); (b) higher magnification SEM microphotographs of quenched needles. (c) FESEM mineral maps on IAP experimental sample A23-016 (2.7 GPa and 1350 °C); (d) and (e) higher magnification SEM microphotographs of melt pools and olivine microcrysts. Colours as in Fig. 2.

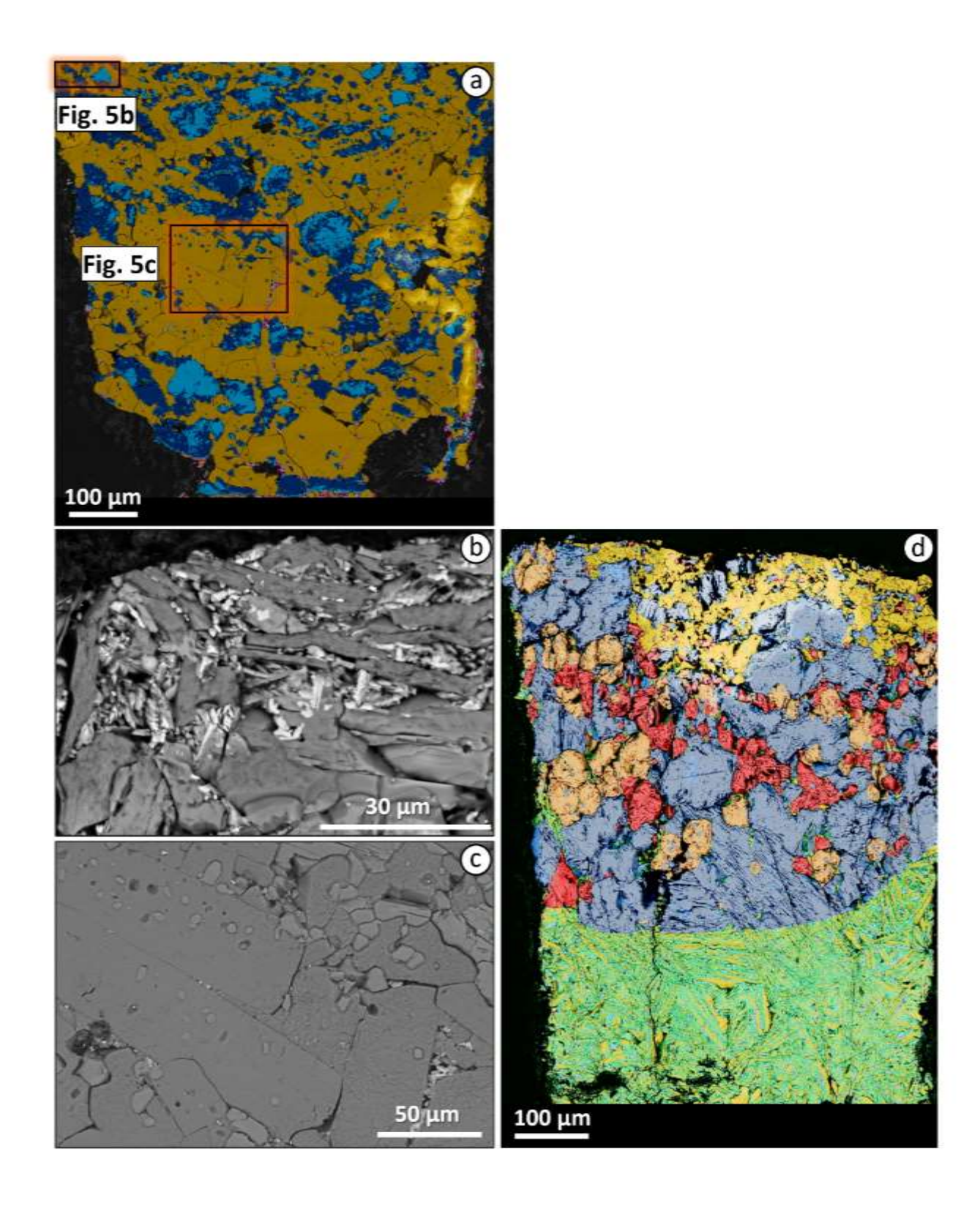


Fig. 5. (a) FESEM mineral maps on IAP experimental sample M22-005 (5 GPa and 1200 °C); (b) and (c) higher magnification SEM microphotographs of quenched needles and olivine microcrysts. (d) FESEM mineral maps on IAP experimental sample M22-010 (5 GPa and 1400 °C). Colours as in Fig. 2.

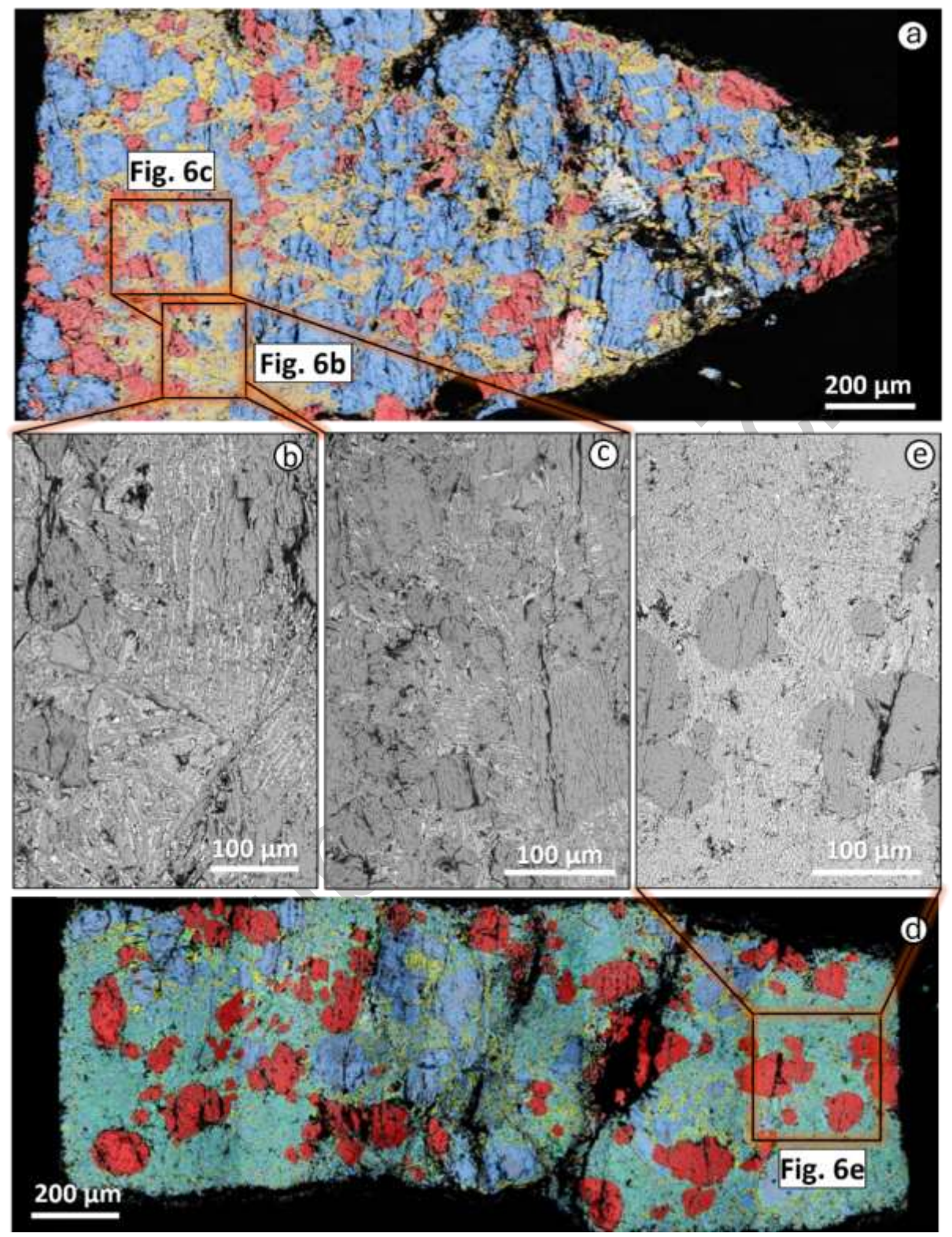


Fig. 6. (a) FESEM mineral maps on APIP experimental sample A23-014 (2.7 GPa and 1300 °C); (b) and (c) Higher magnification SEM microphotographs of quenched needles. (D) FESEM mineral maps on APIP experimental sample A23-019 (2.7 GPa and 1400 °C); (e) Higher magnification SEM microphotographs of melt pools. Colours as in Fig. 2.

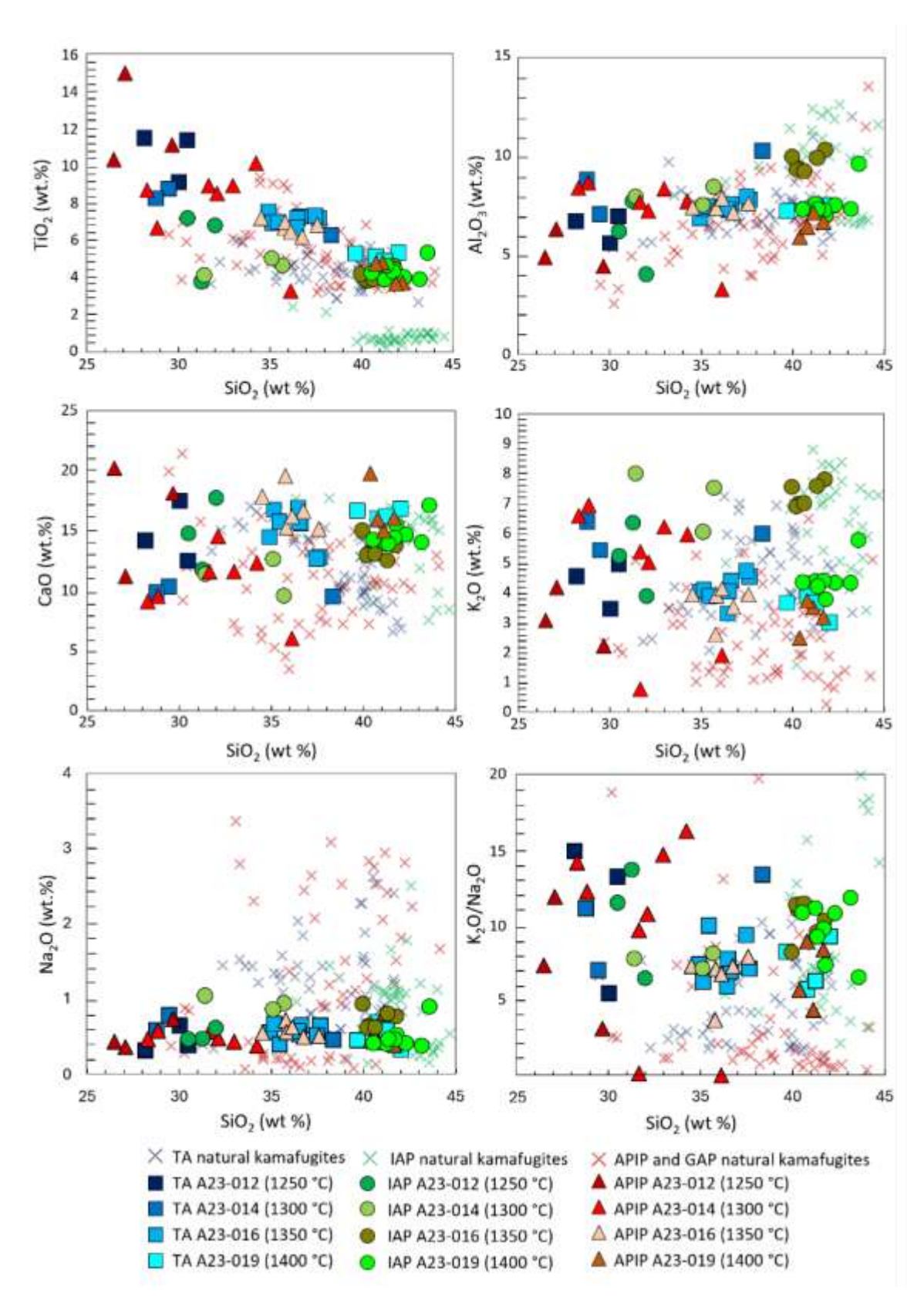


Fig. 7. Harker diagram for major oxides ( $TiO_2$ ,  $Al_2O_3$ , CaO,  $K_2O$ ,  $Na_2O$ ) and  $K_2O/Na_2O$  vs. silica (wt.%) for TA, IAP and APIP experimental glasses at 2.7 GPa. Kamafugites compositions from literature are also plotted for comparative purposes (references in Appendix 1).

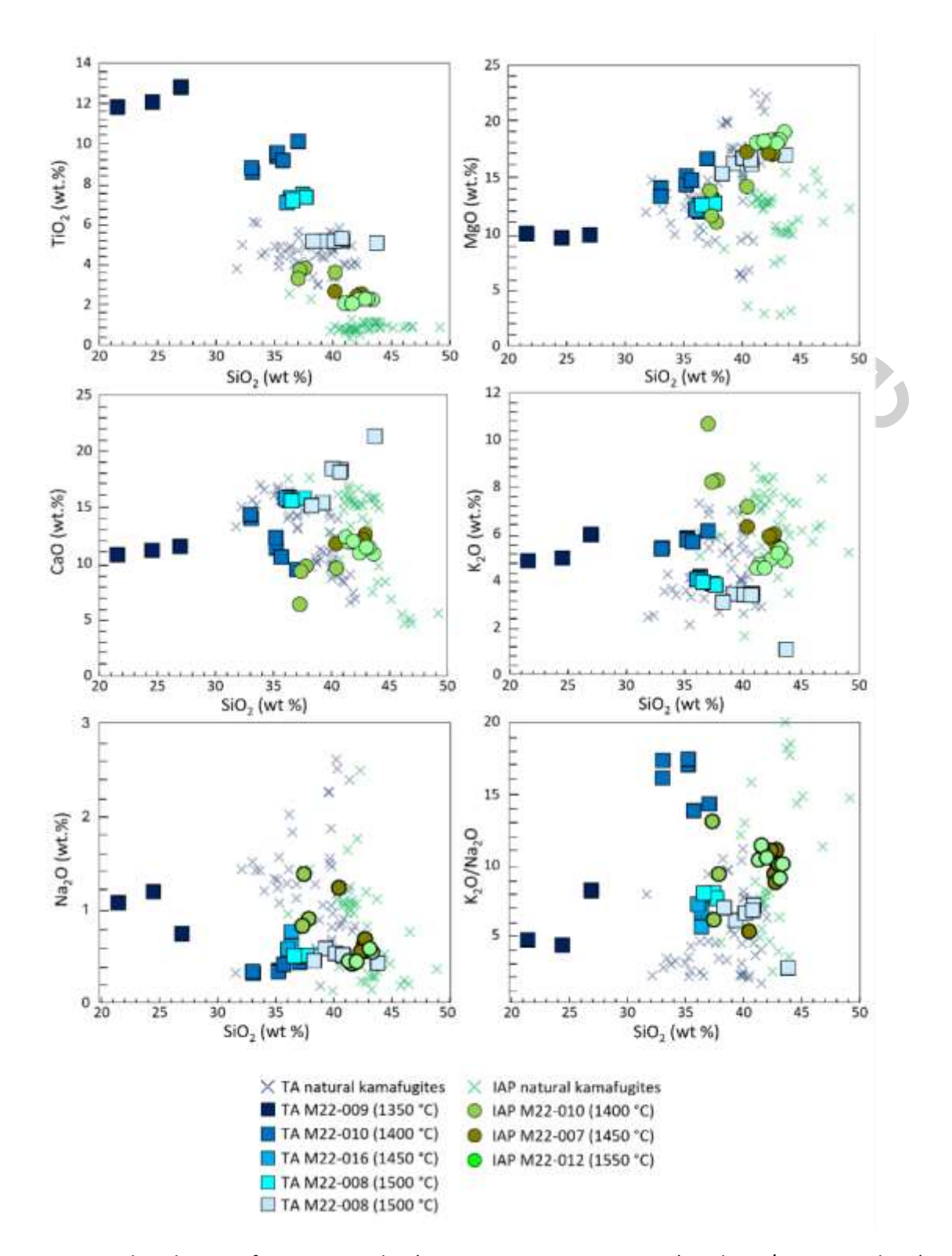


Fig. 8. Harker diagram for major oxides ( $TiO_2$ , MgO, CaO,  $K_2O$ , Na<sub>2</sub>O) and  $K_2O/Na_2O$  vs. silica (wt.%) for TA and IAP experimental glasses at 5 GPa. TA and IAP kamafugite compositions from literature are also plotted for comparison, references as in Fig. 7.

Appendix 1: Quantitative mineral and glass chemical analyses on the experimental samples. Harker diagrams of major oxides vs. SiO<sub>2</sub> (wt.%) are also reported.

**Table 1.** Modal composition (wt.%) of the starting materials for partial melting experiments (Toro Ankole, Alto Paranaiba Igneous Province and Intra-Apennine Province samples) and relative bulk compositions.

	Toro Ankole	Alto Paranaiba Igneous Province	Intra-Apennine Province
Clinopyroxene	60%	50%	40%
Phlogopite (high Ti)	28%	20%	
Phlogopite (low Ti)			55%
Olivine		22%	
Apatite	3%	3%	2%
Ilmenite	2.5%	5%	+ C.N
Magnetite	2.5%		3%
Titanite	4%		
SiO <sub>2</sub>	41.54	41.08	43.93
TiO <sub>2</sub>	5.45	4.37	1.45
$AI_2O_3$	5.45	3.83	6.91
FeO	8.53	9.34	7.56
MnO	0.06	0.09	0.02
MgO	14.06	21.61	19.08
CaO	17.05	13.59	10.63
Na <sub>2</sub> O	0.31	0.26	0.20
K <sub>2</sub> O	2.88	2.06	6.30
$P_2O_5$	1.16	1.16	0.77
$V_2O_5$	0.06	0.05	0.01
Cr <sub>2</sub> O <sub>3</sub>	0.42	0.00	0.68
NiO	0.00	0.08	0.12
Zr <sub>2</sub> O <sub>3</sub>	0.04	0.04	0.03
BaO	0.16	0.14	0.00
Total	97.15	97.69	97.6736

**Table 2.** Summary of all the partial melting experiments that have been run, with relative temperature, pressure, hold time and resulting assemblage.

Experiment	Pressure (GPa)	Temperature (°C)	Hold time (hours)	Phases
			To	oro Ankole Province
A23-008	2.7	1200	12	Cpx 60%, phl 28%, ti 4%, ap 3%, ilm 2.5%, mag 2.5%
A23-012	2.7	1250	12	Melt 20%, cpx 59.6%, phl 16%, ti 0.5%, ap 0.9%, ilm 2.5%, mag 0.5%
A23-014	2.7	1300	12	Melt 37%, ol 9%, cpx 48%, phl 5%, ap 0.9%, ilm 0.1%
A23-016	2.7	1350	12	Melt 63%, cpx 33%, phl 4%
A23-019	2.7	1400	12	Melt 90%, cpx 10%
M22-005	5	1200	10	Melt 1%, cpx 60%, phl 28%, pvk 3%, ap 3%, ilm 2.5%, mag 2.5%
M22-013	5	1250	10	Melt 20%, cpx 47%, phl 15%,tsk 11%, pvk 3%, ap 2%, ilm 2%
M22-009	5	1350	10	Melt 30%, cpx 51%, tsch 14%, phl 3%, Ilm 2%
M22-010	5	1400	10	Melt 58%, cpx 40%, phl 2%
M22-007	5	1450	10	Melt 64%, cpx 36%
M22-008	5	1500	10	Melt 72%, cpx 28%
M22-012	5	1550	10	Melt 85%, cpx 15%
			Alto Pa	ranaiba Igneous Province
A23-008	2.7	1200	12	Cpx 50%, phl 20%, ol 22%, ilm 5%, ap 3%
A23-012	2.7	1250	12	Melt 22.8%, cpx 43.5%, phl 8.3%, ol 25%, ilm 0.4%
A23-014	2.7	1300	12	Melt 31%, cpx 39%, phl 5%, ol 25%
A23-016	2.7	1350	12	Melt 50%, cpx 23%, phl 5%, ol 25%
A23-019	2.7	1400	12	Melt 69%, cpx 10%, ol 21%
			Intr	ra-Apennine Province
A23-008	2.7	1200	12	Cpx 40%, phl 53%, mag 3%, ol 2%, ap 2%
A23-012	2.7	1250	12	Melt 16%, cpx 35%, phl 39%, ol 10%
A23-014	2.7	1300	12	Melt 31%, cpx 33%, phl 26%, ol 10%
A23-016	2.7	1350	12	Melt 69%, cpx 10%, ol 21%
A23-019	2.7	1400	12	Melt 85%, ol 15%
M22-005	5	1200	10	Melt 3%, cpx 40%, phl 50%, mag 3%, ol 2%, ap 2%
M22-013	5	1250	10	Melt 5%, cpx 40%, phl 50%, mag 1%, ol 3%, ap 1%
M22-009	5	1350	10	Melt 5%, cpx 40%, phl 50%, mag 1%, ol 3%, ap 1%
M22-010	5	1400	10	Melt 43%, cpx 38%, phl 7%, ol 10%, tsch 2%
M22-007	5	1450	10	Melt 80%, cpx 10%, ol 10%
M22-008	5	1500	10	Melt 85%, cpx 15%
M22-012	5	1550	10	Melt 90%, cpx 10%

**Table 3.** Averaged chemical composition (SEM and EMP analyses, wt.%) of experimental glasses produced at 2.7 GPa for the three starting materials (Toro Ankole, Alto Paranaiba Igneous Province and Intra-Apennine Province). Values for standard deviation (σ) are given in italics. All data are reported in Electronic Appendix 1.

Experime	Temperatur	Locali	SiO <sub>2</sub>	TiO	Al <sub>2</sub>	FeO	Mn	Mg	CaO	Na <sub>2</sub>	K <sub>2</sub>	P <sub>2</sub>	F	Ва	Sr	Tot	Number of
nt	е	ty		2	O <sub>3</sub>		0	0		0	0	O <sub>5</sub>		0	0	al	analyses
			20	10	C 4			ole Prov		0.4						0.0	
422.042	1250 °C	TA	29.	10.	6.4	14.	0.1	9.8	14.	0.4	4.	4.	0.	0.	0.	96.	3
A23-012			56	69	4	73	7	8	68	4	34	59	43	26	06	26	
G.			1.2 3	1.3	0.7	0.7	0.0	1.0 9	2.5	0.1	0.	0.	0.	0.	0.		
σ			33.	5 7.2	<i>3</i> 9.5	<i>0</i> 11.	3 0.0	12.	<i>3</i> 9.6	<i>7</i> 0.5	<i>78</i> 6.	<i>64</i> 1.	<i>02</i> 0.	<i>04</i> 0.	<i>02</i> 0.	02	
A23-014	1300 °C	TA	55. 55	7. <u>2</u> 8	9.5 6	08	9	80	9.0 7	0.5	20	62	41	30	0.	93. 12	2
A23-014			6.7	1.4	1.0	3.3	0.0	3.8	0.2	0.0	0.	1.	0.	0.	0.	12	
σ			0.7 7	0	3	2	4	3.8	5	9	29	93	20	0. 05	06		
			36.	7.1	7.4	9.5	0.1	11.	15.	0.5	4.	1.	0.	0.	0.	94.	
A23-016	1350 °C	TA	27	5	7	9	3	88	05	6	15	97	16	12	02	51	8
			1.0	0.2	0.3	0.5	0.0	0.7	1.6	0.0	0.	0.	0.	0.	0.		
σ			2	6	3	8	3	7	4	9	44	35	14	10	02		
	1 100 00		40.	5.1	7.3	6.6	0.1	14.	16.	0.5	3.	1.	0.	0.	0.	96.	
A23-019	1400 °C	TA	93	8	8	1	0	72	41	1	57	26	17	11	02	96	4
Ì			0.9	0.2	0.1	0.8	0.0	0.9	0.3	0.1	0.	0.	0.	0.	0.		
σ			8	1	2	3	3	5	7	6	38	28	04	01	02		
					P	Alto Par	anaiba	Igneous	Provin	ce							
	1250 °C	ADID	27.	12.	5.2	13.	0.1	11.	16.	0.5	3.	4.	0.	0.	0.	95.	2
A23-012	1250 °C	APIP	74	18	4	07	8	17	49	0	18	82	31	24	08	19	3
Ì			1.6	2.4	0.9	1.7	0.0	1.8	4.7	0.2	0.	1.	0.	0.	0.		
σ			9	9	7	4	5	0	1	0	98	65	12	05	04		
Ì	1300 °C	APIP	33.	9.2	7.7	10.	0.1	10.	12.	0.4	5.	2.	0.	0.	0.	94.	3
A23-014	1300 C	AI II	10	2	9	85	2	91	79	2	75	64	52	26	06	44	3
Ì			1.0	0.8	0.5	0.4	0.0	0.5	1.5	0.0	0.	0.	0.	0.	0.		
σ			7	4	5	9	3	7	3	5	63	68	05	04	01		
	1350 °C	APIP	36.	6.7	7.4	9.1	0.1	11.	16.	0.5	3.	1.	0.	0.	0.	94.	6
A23-016			09	3	9	0	4	58	75	7	69	98	25	16	03	57	
ı _			1.0	0.3	0.2	0.6	0.0	1.0	1.6	0.0	0.	0.	0.	0.	0.		
σ			3	5	4	1	3	8	9	8	56	33	06	03	03	0.5	
A 2 2 0 1 0	1400 °C	APIP	40.	4.5	6.5 5	5.9	0.1	15.	16.	0.5	3.	1.	0.	0.	0.	95.	4
A23-019			98 <i>0.5</i>	3 <i>0.4</i>	0.5	0 0.5	0.0	0.8	68 2.1	1 0.2	24 <i>0</i> .	30 <i>0.</i>	12	12 <i>0</i> .	05 <i>0.</i>	52	
σ			<i>0.5</i>	0.4 7	0.5	2	0.0	0.8	2.1 1	0.2	<i>0.</i> 54	0. 86	0. 03	0. 03	0. 02		
0			3		1	_		nine Pro		- 0	54	00	03	03	02		
			31.	5.9	6.0	10.	0.1	13.	14.	0.5	5.	5.	0.	0.	0.	93.	
A23-012	1250 °C	IAP	25	3.9	0.0	48	5	13. 13	73	0.5	5. 18	5. 50	0. 39	0. 15	10	93. 51	3
74J-014			0. <i>7</i>	1.8	1.8	1.6	0.0	2.4	2.9	0.0	1.	0.	0.	0.	0.	31	
σ			5	7.0	5	3	5	8	2. <i>3</i>	8	23	69	03	0. 04	0. 03		
ı			34.	4.6	7.9	9.7	0.1	10.	11.	0.9	7.	2.	0.	0.	0.	89.	
A23-014	1300 °C	IAP	06	2	9	3.7	2	50	18	4	21	90	48	17	07	99	3
			2.3	0.4	0.4	1.2	0.0	0.7	1.5	0.0	1.	0.	0.	0.	0.		
σ			2	6	6	3	5	1	4	9	02	73	09	04	05		
1	1250.85		40.	4.2	9.8	6.2	0.0	9.6	13.	0.7	7.	1.	0.	0.	0.	93.	_
A23-016	1350 °C	IAP	77	1	5	8	9	0	36	3	40	34	21	07	03	94	7
) 			0.6	0.3	0.5	0.2	0.0	2.6	0.8	0.1	0.	0.	0.	0.	0.		
σ			8	5	4	6	3	6	1	2	40	05	21	07	03		
	1400 %	IAD	41.	4.3	7.6	6.4	0.0	13.	14.	0.4	4.	1.	0.	0.	0.	95.	C
A23-019	1400 °C	IAP	96	6	4	5	9	85	69	9	46	80	16	08	03	33	8
			1.0	0.4	0.8	0.5	0.0	3.1	1.0	0.1	0.	0.	0.	0.	0.	0.9	
σ	~		2	7	2	2	3	3	9	7	57	35	10	06	03	39	

**Table 4.** Averaged chemical composition (SEM and EMP analyses, wt.%) of experimental clinopyroxene, phlogopite and olivine at 2.7 GPa for the three samples (Toro Ankole, Alto Paranaiba Igneous Province and Intra-Apennine Province). Values for standard deviation (σ) are given in italics . All data are reported in Electronic Appendix 1.

Experiment	Phase	Temperature	SiO <sub>2</sub>	TiO <sub>2</sub>	$Al_2O_3$	FeO	MnO	MgO	CaO	Na₂O	K <sub>2</sub> O	P <sub>2</sub> O <sub>5</sub>	Cr <sub>2</sub> O <sub>3</sub>	NiO	$V_2O_5$	BaO	Total	Number of analyses
						To	oro Anko	le Provinc	e									
A23-012	Clinopyroxene	1250 °C	50.01	1.93	3.81	5.35	0.05	14.35	22.85	0.45							98.80	3
σ			0.59	0.15	0.79	0.79	0.09	0.82	0.86	0.10								
A23-014	Clinopyroxene	1300 °C	50.04	1.99	5.74	4.05		15.29	22.22	0.33	0.04						99.70	5
σ			0.82	0.26	0.91	0.15		0.44	0.53	0.19	0.08							
A23-016	Clinopyroxene	1350 °C	50.87	1.56	4.12	3.56	0.02	16.42	22.52	0.08	0.03						99.16	6
σ			0.72	0.23	0.54	0.23	0.03	0.41	0.38	0.12	0.04							
A23-019	Clinopyroxene	1400 °C	52.56	0.95	2.99	2.98		17.18	22.72	- 4	<b></b> Y						99.38	3
σ			1.25	0.16	0.61	0.28		0.62	0.22	(	1-							
A23-012	Phlogopite	1250 °C	37.40	6.10	14.80	7.73		18.31	7.		10.22				0.19	0.61	95.34	3
σ	· ·		0.56	0.35	0.05	0.11		0.42			0.22				0.04	0.04		
A23-014	Phlogopite	1300 °C	36.76	7.22	13.86	10.46		16.44	0.54		9.97				0.13	0.53	95.91	1
A23-016	Phlogopite	1350 °C	35.55	9.39	11.47	10.39	0.05	16.19	3.17	<b>/</b>	8.44	0.29			0.17	0.49	95.60	3
σ	· ·		3.30	2.16	2.14	2.90	0.09	2.12	2.90		2.20	0.51			0.03	0.08		
A23-014	Olivine	1300 °C	39.08	0.14	0.02	15.50	0.15	43.61	0.76					0.01			99.27	5
σ			0.58	0.06	0.04	0.62	0.03	0.29	0.51					0.01				_
							-	gneous Pr										
A23-012	Clinopyroxene	1250 °C	50.22	1.59	4.45	4.43	0.07	15.07	22.43	0.42	0.08	0.05					98.80	3
σ			2.19	0.91	1.52	0.84	0.06	1.60	0.66	0.02	0.13	0.08						
A23-014	Clinopyroxene	1300 °C	49.89	1.91	5.31	4.04	0.06	15.34	22.36	0.09	0.03						99.03	5
σ	······································		0.79	0.13	0.59	0.22	0.06	0.56	0.28	0.19	0.06							
A23-016	Clinopyroxene	1350 °C	51.91	1.35	3.46	3.48	0.03	16.86	22.34	0.11	0.02						99.54	8
σ			0.70	0.19	0.56	0.26	0.04	0.40	0.42	0.15	0.04							
A23-019	Clinopyroxene	1400 °C	52.56	1.10	2.77	3.13	0.00	17.39	22.72	0.11	0.11						99.89	3
σ			1.07	0.39	0.78	0.46	0.00	0.74	0.67	0.20	0.10							
A23-012	Phlogopite	1250 °C	36.20	6.91	13.92	7.41		19.23	0.16		9.86				0.13	0.34	94.15	3
σ	oBobite	1200 0	1.74	1.84	1.27	2.30		0.59	0.27		0.55				0.08	0.29	525	J
A23-014	Phlogopite	1300 °C	35.88	7.58	12.98	10.06	0.04	16.55	1.83		9.35	0.53			0.11	0.38	95.28	3
σ	·8-1		1.45	0.43	0.39	0.17	0.06	0.77	2.60		0.70	0.92			0.10	0.34		_
A23-016	Phlogopite	1350 °C	38.38	7.56	11.97	9.03	0.04	16.95	1.61		9.26				0.16	0.46	95.41	3
σ	oBobite	2000	0.03	0.45	1.13	1.21	0.06	1.49	1.66		0.86				0.01	0.03	551.12	J
A23-012	Olivine	1250 °C	39.09	0.13		14.81	0.17	43.72	0.31		0.02			0.10			98.33	3
7		3233	0.66	0.12		1.50	0.03	0.88	0.09		0.03			0.17			30.00	ū
A23-014	Olivine	1300 °C	39.52	0.11		14.20	0.16	45.65	0.37								100.00	4
7		2000 0	0.46	0.03		0.09	0.01	0.63	0.02									•
A23-016	Olivine	1350 °C	40.19	0.03	0.02	9.97	0.13	48.76	0.38				0.01	0.17			99.74	7
5	J., VIII C	1550	0.79	0.16	0.02	1.32	0.02	1.22	0.29				0.02	0.17			33.7 1	,
A23-019	Olivine	1400 °C	40.42	0.10	0.03	8.02	0.02	50.12	0.25				0.02	0.03			99.23	7
723-019	CHVIIIC	1400 C	0.41	0.07	0.03	0.39	0.04	0.83	0.40				0.02	0.03			JJ.23	,
,			0.41	0.03	0.04			ine Provir					0.02	0.00				

A23-012	Clinopyroxene	1250 °C	52.47	0.56	2.72	3.63		16.64	21.93	0.43	0.23						98.53	3
σ			0.29	0.01	0.21	0.05		0.35	0.31	0.01	0.00							
A23-014	Clinopyroxene	1300 °C	52.85	0.65	2.66	3.73	0.04	17.04	21.77	0.22	0.19	0.13					99.27	5
σ			0.57	0.14	0.18	0.27	0.06	0.47	0.54	0.20	0.33	0.08						
A23-016	Clinopyroxene	1350 °C	52.85	0.51	2.56	2.50	0.02	17.78	22.18		0.04		/				98.44	6
σ			0.59	0.03	0.14	0.13	0.04	0.26	0.46		0.07		(					
A23-019	Clinopyroxene	1400 °C	49.68	0.37	1.63	4.06	0.03	29.20	14.47					<b>4-</b> )			99.44	3
σ			7.83	0.32	1.41	2.94	0.05	17.60	12.17			70						
A23-014	Phlogopite	1300 °C	39.52	3.62	14.39	5.27		22.03			10.59				0.02	0.12	95.55	9
σ			0.81	0.73	0.60	0.29		1.12			0.48	-			0.05	0.18		
A23-016	Phlogopite	1350 °C	40.11	4.77	12.07	5.87		18.98	3.39		10.13	0.20			0.04	0.07	95.63	4
σ			1.19	0.40	0.88	0.11		1.71	2.01		0.36	0.41			0.07	0.14		
A23-014	Olivine	1300 °C	39.53	0.07		13.60	0.15	45.91	0.38		0.02	()		0.06			99.72	3
σ			0.57	0.06		0.22	0.01	0.66	0.03		0.04			0.11				
A23-016	Olivine	1350 °C	40.42	0.05	0.02	7.84	0.07	50.68	0.43	-(	0.03		0.04	0.00			99.58	8
σ			1.08	0.05	0.03	0.24	0.00	1.16	0.07	2. /	0.06		0.04	0.01				
A23-019	Olivine	1400 °C	40.78	0.04	0.03	7.76	0.08	50.27	0.45		0.00		0.03	0.03			99.46	6
σ			0.582	0.04	0.03	0.81	0.02	0.59	0.06		0.00		0.03	0.07				

**Table 5**. Averaged chemical composition (SEM and EMP analyses, wt.%) of experimental glasses at 5 GPa for the two samples (Toro Ankole and Intra-Apennine Province). Values for standard deviation (σ) are given in italics. All data are reported in Electronic Appendix 1.

Experiment	Temperature	Locality	SiO <sub>2</sub>	TiO <sub>2</sub>	$Al_2O_3$	FeO	MnO	MgO	CaO	Na₂O	K <sub>2</sub> O	$P_2O_5$	F	BaO	SrO	Cr <sub>2</sub> O <sub>3</sub>	Total	Number of analyses
							Toro A	nkole Pro	vince									
M22-013	1250 °C	TA	26.70	10.20	4.96	17.11	0.20	9.19	13.92	0.37	5.53	5.23	0.51	0.38	0.09		94.39	3
σ			0.97	0.31	0.16	0.11	0.03	0.46	0.72	0.01	0.28	0.19	0.01	0.04	0.03			
M22-009	1350 °C	TA	24.36	12.24	5.86	10.85		9.85	11.15	1.00	5.26	6.54					87.12	3
σ			2.71	0.51	0.23	0.69		0.19	0.37	0.23	0.61	0.76	<	-				
M22-010	1400 °C	TA	34.88	9.27	8.62	4.56	0.10	14.74	12.01	0.36	5.68	1.88	0.19	0.19	0.03		92.52	6
σ			1.55	0.55	0.43	0.33	0.05	1.14	1.92	0.05	0.29	0.55	0.15	0.15	0.03			
M22-007	1450 °C	TA	36.28	7.23	7.14	11.89	0.14	12.24	15.77	0.65	4.12	1.79	0.42	0.22	0.04		97.94	4
σ			0.14	0.11	0.07	0.15	0.01	0.27	0.11	0.08	0.05	0.06	0.09	0.01	0.01			
M22-008	1500 °C	TA	37.21	7.33	7.05	9.86	0.10	12.76	15.72	0.50	3.87	1.82					96.22	3
σ			0.58	0.15	0.05	0.18	0.09	0.18	0.12	0.01	0.06	0.09						
M22-012	1550 °C	TA	40.49	5.17	6.81	4.09	0.06	16.36	17.82	0.50	2.97	1.19	0.07	0.13	0.03		95.60	6
σ			1.85	0.07	0.34	0.33	0.05	0.58	2.28	0.06	0.94	0.18	0.06	0.04	0.02			
							Intra-Ap	ennine Pr	ovince									
M22-010	1400 °C	IAP	37.87	3.56	7.90	9.04	0.05	12.62	8.81	0.79	8.86	1.41	0.22	0.04	0.02		91.21	5
σ			1.51	0.22	0.55	0.77	0.05	1.39	1.39	0.50	1.41	0.94	0.30	0.06	0.03			
M22-007	1450 °C	IAP	42.28	2.47	8.07	5.34	0.06	17.37	12.03	0.68	5.91	1.16	0.38	0.06	0.04		95.85	7
σ			0.85	0.11	0.12	0.24	0.03	0.46	0.31	0.25	0.24	0.15	0.06	0.01	0.02			
M22-012	1550 °C	IAP	42.06	2.14	7.08	5.38	0.08	18.17	11.89	0.47	4.84	0.56	0.11	0.05	0.03	0.055	92.92	6
σ			0.86	0.11	0.03	0.38	0.03	0.12	0.36	0.07	0.35	0.29	0.09	0.04	0.03	0.09		

**Table 6.** Averaged chemical composition (SEM and EMP analyses, wt.%) of experimental clinopyroxene, phlogopite, olivine and tschermakite at 5 GPa for the two samples (Toro Ankole and Intra-Apennine Province). Values for standard deviation (σ) are given in italics. All data are reported in Electronic Appendix 1.

Experiment	Phase	Temp.	SiO <sub>2</sub>	TiO <sub>2</sub>	Al <sub>2</sub> O <sub>3</sub>	FeO	MnO	MgO	CaO	Na <sub>2</sub> O	K₂O	P <sub>2</sub> O <sub>5</sub>	Cr <sub>2</sub> O <sub>3</sub>	NiO	V <sub>2</sub> O <sub>5</sub>	ВаО	Pm <sub>2</sub> O <sub>3</sub>	Ta₂O₅	Total	Number of analyses
							7	Toro A	Ankole Pro	vince										
M22-013	Clinopyroxene	1250 °C	54.59	0.57	1.41	3.83		18.09	19.93	0.72									98.09	3
σ			0.65	0.10	1.23	0.44		0.92	0.73	0.06										
M22-009	Clinopyroxene	1350 °C	53.03	1.32	1.04	3.70		16.74	21.83	0.16									97.81	4
σ			1.50	0.07	2.08	0.21		0.94	0.42	0.32										
M22-010	Clinopyroxene	1400 °C	51.99	1.10	4.78	1.92		18.02	20.08	0.49	0.15								98.52	5
σ			0.84	0.39	0.36	0.24		0.79	1.47	0.09	0.01									
M22-007	Clinopyroxene	1450 °C	51.57	0.93	5.05	3.48		16.17	21.72	0.46	0.17								99.56	3
σ			1.00	0.11	0.33	0.02		0.49	0.18	0.02	0.02									
M22-008	Clinopyroxene	1500 °C	51.94	0.84	4.34	3.08		16.14	22.99	0.40	0.06								99.80	5
σ			0.69	0.08	0.41	0.28		0.29	0.42	0.03	0.09									
M22-013	Phlogopite	1250 °C	41.03	1.52	13.11	4.60		23.45			9.88								93.59	1
M22-009	Phlogopite	1350 °C	39.12	4.55	14.57	5.72		20.62			10.81								95.39	3
σ			0.56	0.03	0.45	0.13		0.47			0.30									
M22-010	Phlogopite	1400 °C	38.63	6.20	13.41	5.29	0.10	21.70	2.13		9.49	1.37			0.18	0.55			99.05	1

M22-013	Tschermakite	1250 °C	37.85	2.86	18.45	12.21	0.37	8.67	17.07				0.04						97.52	5
σ			0.62	0.30	0.70	1.64	0.07	0.44	1.15				0.06							
M22-009	Tschermakite	1350 °C	39.58	2.91	19.88	8.36	0.11	13.64	13.42				0.06				0.38	0.38	98.67	4
σ			0.55	0.20	0.64	0.45	0.13	0.24	0.69				0.03				0.43	0.75		
								Intra-A	oennine P	rovince										
M22-009	Clinopyroxene	1350 °C	53.62	0.72	2.66	4.06		16.45	21.27	0.32				-	/	4			99.08	2
σ			2.17	0.04	3.76	0.01		1.46	0.78	0.45						)				
M22-010	Clinopyroxene	1400 °C	53.13	0.40	3.38	3.17	0.02	17.82	20.65	0.50	0.23	0.21							99.52	4
σ			0.49	0.05	0.22	0.04	0.05	0.22	0.35	0.03	0.02	0.02	<b>&gt;</b>		-					
M22-007	Clinopyroxene	1450 °C	53.51	0.26	3.14	2.40		20.15	18.46	0.32	0.21	0.30	-		) <u></u>				98.73	4
σ			0.39	0.03	0.47	0.18		0.66	0.20	0.21	0.03	0.04	<b>X</b> \	-						
M22-008	Clinopyroxene	1500 °C	53.84	0.25	2.67	1.46		20.80	19.42	0.24	0.22	, (	0.25						98.90	3
σ			0.45	0.01	0.09	0.06		0.38	0.67	0.21	0.02									
M22-012	Clinopyroxene	1550 °C	53.99	0.55	2.94	1.40		18.99	22.10	0.15									#####	4
σ			0.52	0.05	0.29	0.31		0.26	0.13	0.17	(		-							
M22-009	Phlogopite	1350 °C	39.91	2.25	13.65	6.11		21.92			10.78								94.61	3
σ			0.60	0.11	0.71	0.16		0.09			0.40									
M22-010	Phlogopite	1400 °C	40.55	2.35	14.52	4.19		23.28			10.93								95.82	4
σ			0.22	0.08	0.12	0.11		0.15			0.39									
M22-009	Olivine	1350 °C	39.35	0.09		16.15	0.11	42.71			0.12								98.61	3
σ			1.51	0.08		0.50	0.09	0.67	0.15		0.21									
M22-010	Olivine	1400 °C	40.46			9.67	0.04	49.16	0.21	0.08	0.103			0.04					99.67	5
σ			0.66			2.20	0.05	2.12	0.12	0.05				0.09						
M22-007	Olivine	1450 °C	40.97	0.01	0.02	5.61	0.01	52.66	0.31				0.02						99.61	5
σ			0.16	0.03	0.04	0.12	0.03	0.13	0.04				0.50							
M22-010	Tschermakite	1400 °C	39.44	1.09	20.85	6.23	0.13	17.44	9.96				0.55						95.63	6
σ			1.20	0.10	0.77	0.68	0.03	0.55	0.82											